Centro de Investigación Científica y de Educación Superior de Ensenada, Baja California

Maestría en Ciencias

en Ciencias de la Tierra con orientación en Geofísica Aplicada

---

Extensional waves in a fluid-saturated porous cylinder with an impermeable radial surface

Tesis

para cubrir parcialmente los requisitos necesarios para obtener el grado de

Maestro en Ciencias

Presenta:

Josué Gabriel González Flores

Ensenada, Baja California, México

2017

Tesis defendida por

Josué Gabriel González Flores

y aprobada por el siguiente Comité

Dr. Pratap Narayan Sahay Sahay

Director del Comité

Dr. Jonás de Dios De Basabe Delgado

Dr. Markus Sebastian Gross

Dr. Juan García Abdeslem

Coordinador del Programa de Posgrado en Ciencias de la Tierra

---

Dra. Rufina Hernández Martínez

Director de Estudios de Posgrado

Resumen de la tesis que presenta Josué Gabriel González Flores como requisito parcial para la obtención del grado de Maestro en Ciencias en Ciencias de la Tierra con orientación en Geofísica Aplicada.

Ondas extensionales en un cilindro poroso saturado con superficie radial impermeable

Resumen aprobado por:

Dr. Pratap Narayan Sahay Sahay
Director de tesis

Los estudios de onda extensional son un área activa de investigación experimental para la caracterización de los módulos elásticos de materiales porosos saturados en el régimen de bajas frecuencias (sub 100Hz). En estos estudios, un núcleo cilíndrico de longitud finita es excitado en un modo característico de onda longitudinal estacionaria. El problema de valor de frontera asociado con las oscilaciones extensionales de un cilindro poroso saturado, para el caso de la superficie radial libre de tracción con poros abiertos, se ha analizado completamente analíticamente. Sin embargo, su contra parte de poros cerrados libre de tracción, en la que la superficie radial está sellada de tal manera que el fluido no puede moverse fuera de la muestra, no ha sido analizada analíticamente completamente. Aún así, los estudios experimentales con superficie cerrada son un área importante de la investigación para entender la atenuación sísmica en rocas porosas. Con base en la teoría dCS de poroelasticidad, el problema de valor en la frontera del movimiento extensional de un cilindro poro con superficie radial impermeable libre de esfuerzos es analizado en este trabajo. Las condiciones en la superficie radial se consideran como: i) las tracciones correspondientes a la suma total de esfuerzos en las partes sólida y fluida son iguales a cero, ii) el movimiento relativo es nulo entre las fases en la dirección normal y, iii) sin esfuerzo interno en la dirección tangencial. La relación de dispersión muestra que un cilindro poroso saturado aparte de comportarse como un sólido elástico efectivo no drenado, como es considerado en la comunidad experimental, tiene otros dos modos altamente disipativos. Debido a la presión de confinamiento aplicada para sellar un cilindro poroso en un experimento de baja frecuencia, el cilindro es forzado a oscilar bajo las condiciones de esfuerzo en su superficie radial. Por lo tanto, aparte de la excitación del primer modo extensional, los otros dos modos naturales también deben ser inducidos en la muestra. Por lo que, la atenuación observada en los experimentos puede ser explicada por la presencia de los dos adicionales modos altamente atenuados.

Palabras Clave: **poroelasticidad, atenuación de ondas, ondas extensionales**

Abstract of the thesis presented by Josué Gabriel González Flores as a partial requirement to obtain the Master of Science degree in Master in Earth Science with orientation in Applied Geophysics.

Extensional waves in a fluid-saturated porous cylinder with an impermeable radial surface

Abstract approved by:

Dr. Pratap Narayan Sahay Sahay
Thesis Director

Extensional wave studies are an active area of experimental research for the characterization of the elastic moduli of fluid-saturated porous materials in low frequency regime (sub 100Hz). Herein, a cylindrical core of finite length is excited into a characteristic mode of a longitudinal standing wave. The boundary-value problem associated with extensional oscillations of a fluid-saturated porous circular cylinder, for the case of traction-free open-pore radial surface, is analytically analyzed. However, its traction-free closed-pore counterpart, wherein the radial surface is sealed such that the fluid cannot move out of the sample, has not been analytically analyzed properly yet. Although, experimental studies with surface pores being held closed are a major area of research to understand seismic attenuation in porous rocks. Based on the dCS framework of poroelasticity, the boundary-value problem of extensional motion of a porous cylinder with a stress-free impermeable radial surface is analyzed in this work. The conditions on the radial surface are taken as (i) the tractions corresponding to the sum total of phasic stresses vanishing, (ii) vanishing relative motion between the phases in the normal direction and, (iii) no internal stress in the tangential direction. The dispersion relation shows that a saturated porous cylinder, apart from vibrating as an effective undrained elastic solid, as considered in the experimental community, has additional two modes and they are highly dissipative. Due to the confining pressure applied to seal the sample in a low frequency experiment (LF), the porous cylinder is subjected to forced oscillations under the condition of non-vanishing stresses at its impermeable radial surface. Therefore, in addition to the excitation of the mode of effective undrained elastic solid, the other two natural modes ought to be induced also. Then, the observed attenuation in a LF experiment can be explained on account of the presence of these two additional highly attenuated modes.

Keywords: **poroelasticity, wave attenuation, extensional waves**

Dedicatoria

A Dios, mi esposa y mis padres

Agradecimientos

Al Centro de Investigación Científica y de Educación Superior de Ensenada (CICESE).

Al Consejo Nacional de Ciencia y Tecnología (CONACyT) por brindarme el apoyo económico para la realización de este proyecto como becario No. 587208.

Al Dr. Pratap Sahay por su constante apoyo y atención, a mis sinodales el Dr. Jonás D. de Basabe y Dr. Markus Gross por su tiempo y observaciones para la mejora de mi trabajo.

A mi esposa Stephany por su paciencia, amor y constantes atenciones.

A mis compañeros de laboratorio Ana, Gabriel y Gautier por sus enseñanzas y amistad.

A mis compañeros del grupo de física de rocas, Iván y Bety, por sus comentarios y observaciones.

Al personal administrativo de CICESE, por su atención y orientación.

Contents

Page

List of figures

List of tables

Tables of notation

Table 1: Phasic field quantities

$\hat{\mathbf{e}}_j$		unit vector in jth direction
$\mathbf{u}^{\mathrm{s}}$	$= \hat{\mathbf{e}}_j \mathrm{u}^{\mathrm{s}}_j$	averaged displacement field vector of solid-frame
$\mathrm{u}^{\mathrm{s}}_{jk}$	$= \frac{1}{2}(\mathrm{u}^{\mathrm{s}}_{j,k} + \mathrm{u}^{\mathrm{s}}_{k,j})$	solid-frame strain tensor
$\breve{\mathrm{u}}^{\mathrm{s}}_{jk}$	$= \mathrm{u}^{\mathrm{s}}_{jk} - \frac{1}{3}\mathrm{u}^{\mathrm{s}}_{ll}\delta_{jk}$	trace-free part of solid-frame strain tensor
$\mathbf{u}^{\mathrm{f}}$	$= \hat{\mathbf{e}}_j \mathrm{u}^{\mathrm{f}}_j$	averaged displacement field vector of fluid
$\mathrm{v}^{\mathrm{f}}_j$	$= \partial_t \mathrm{u}^{\mathrm{f}}_j$	averaged velocity field vector of fluid
$\mathrm{v}^{\mathrm{f}}_{jk}$	$= \frac{1}{2}(\mathrm{v}^{\mathrm{f}}_{j,k} + \mathrm{v}^{\mathrm{f}}_{k,j})$	fluid (macroscopic) strain-rate tensor
$\breve{\mathrm{v}}^{\mathrm{f}}_{jk}$	$= \mathrm{v}^{\mathrm{s}}_{jk} - \frac{1}{3}\mathrm{v}^{\mathrm{s}}_{ll}\delta_{jk}$	trace-free part of macro. fluid strain-rate tensor
ζ	$= -\eta_{_0}(\mathrm{u}^{\mathrm{f}}_{jj} - \mathrm{u}^{\mathrm{s}}_{jj})$	increase of fluid content
τ^{s}_{jk}	$= (1-\eta_0)\sigma^{\mathrm{s}}_{jk}$	solid stress tensor per unit vol. of porous medium
τ^{f}_{jk}	$= \eta_0 \sigma^{\mathrm{f}}_{jk}$	fluid stress tensor per unit vol. of porous medium
p^{f}	$= -\frac{1}{3\eta_0}\tau^{\mathrm{f}}_{jj}$	macroscopic fluid pressure
σ^{s}_{jk}		macro. solid stress tensor per unit vol. of solid phase
σ^{f}_{jk}		macro. fluid stress tensor per unit vol. of fluid phase

Table 2: Natural dynamical fields

$\mathrm{u}^{\mathrm{m}}_j$	$= \mathrm{m}_{\mathrm{s}}\mathrm{u}^{\mathrm{s}}_j + \mathrm{m}_{\mathrm{f}}\mathrm{u}^{\mathrm{f}}_j$	center-of-mass or mean displacement field
$\mathrm{u}^{\mathrm{i}}_j$	$= \mathrm{m}_{\mathrm{d}}(\mathrm{u}^{\mathrm{f}}_j - \mathrm{u}^{\mathrm{s}}_j)$	internal rotational field
$\mathrm{u}^{\mathrm{m}}_{jk}$	$= \mathrm{m}_{\mathrm{s}}\mathrm{u}^{\mathrm{s}}_{jk} + \mathrm{m}_{\mathrm{f}}\mathrm{u}^{\mathrm{f}}_{jk}$	centre-of-mass or mean field strain tensor
$\mathrm{u}^{\mathrm{i}}_{jk}$	$= \mathrm{m}^{\mathrm{d}}(\mathrm{u}^{\mathrm{f}}_{jk} - \mathrm{u}^{\mathrm{s}}_{jk})$	internal rotational field strain tensor
$\breve{\mathrm{u}}^{\mathrm{m}}_{jk}$	$= \mathrm{u}^{\mathrm{m}}_{jk} - \frac{1}{3}\mathrm{u}^{\mathrm{m}}_{ll}\delta_{jk}$	trace-free part of centre-of-mass or mean field strain tensor
$\breve{\mathrm{u}}^{\mathrm{i}}_{jk}$	$= \bar{\mathrm{u}}^{\mathrm{i}}_{jk} - \frac{1}{3}\bar{\mathrm{u}}^{\mathrm{i}}_{ll}\delta_{jk}$	trace-free part of internal rotational field strain tensor
τ^{m}_{jk}	$= \tau^{\mathrm{s}}_{jk} + \tau^{\mathrm{f}}_{jk}$	total stress tensor of porous medium per unit volume
τ^{i}_{jk}	$= \frac{1}{\mathrm{m}_{\mathrm{d}}}(\mathrm{m}^{\mathrm{s}}\tau^{\mathrm{f}}_{jk} - \mathrm{m}^{\mathrm{f}}\tau^{\mathrm{s}}_{jk})$	internal / couple-stress tensor of porous medium per unit volume

Table 3: End members (microscopic) parameters

$\rho_{\mathrm{s}}^{\circ}$	solid unperturbed density
$\rho_{\mathrm{f}}^{\circ}$	pore fluid unperturbed density
$\mathrm{K_s}$	solid-mineral bulk modulus
μ_{s}	solid-mineral shear modulus
$\mathrm{K_f}$	pore fluid bulk modulus
ξ_{f}	pore fluid bulk viscosity
μ_{f}	pore fluid shear viscosity

Table 4: Frame (macroscopic) parameters

$\eta_{_0}$		unperturbed porosity
$\phi_{_0}$	$\eta_{_0} + \phi_{_0} = 1$	unperturbed volume fraction of solid
K		permeability
S	> 1	tortuosity factor
$\delta_{_{\mathrm{K}}}$	$0 \leq \delta_{_{\mathrm{K}}} \leq 1$	bulk modulus decrement parameter of solid-frame
δ_{μ}	$0 \leq \delta_{\mu_{\mathrm{s}}} \leq 1$	shear modulus decrement parameter of solid-frame
n	$0 \leq n \leq \frac{1}{\delta_{\mathrm{K}}}$	micro-inhomogeneity parameter

Table 5: Derived parameters

α	$= \eta_0 + \phi_0\ \delta_{\mathrm{K}}$	Biot bulk coefficient
	$= 1 - \frac{\mathrm{K}_0}{\mathrm{K}_\mathrm{s}}$	
$\alpha^\star$	$= \eta_0 + \phi_0\ \delta_{\mathrm{K}}\ n$	effective pressure coefficient for bulk volume
χ	$= \eta_0 + \phi_0\ \mathrm{n}$	effective pressure coefficient for pore-volume
$\mathrm{M}^\star$	$= (\frac{\eta_0}{\mathrm{K}_\mathrm{f}} + \frac{\alpha^\star - \eta_0}{\mathrm{K}_\mathrm{s}})^{-1}$	generalized fluid storage coefficient
	$= (\frac{\eta_0}{\mathrm{K}_\mathrm{f}} + \mathrm{n}\frac{\alpha - \eta_0}{\mathrm{K}_\mathrm{s}})^{-1}$	
α_μ	$= \eta_0 + \phi_0\delta_\mu$	Shear coefficient
	$= 1 - \frac{\mu_0}{\mu_\mathrm{s}}$	
K_0	$= \phi_0(1 - \delta_{\mathrm{K}})\mathrm{K}_\mathrm{s}$	dry solid-frame bulk modulus
	$= (1 - \alpha)\mathrm{K}_\mathrm{s}$	
μ_0	$= \phi_0(1 - \delta_\mu)\mu_\mathrm{s}$	dry solid-frame shear modulus
	$= (1 - \alpha_\mu)\mu_\mathrm{s}$	
ρ^0_m	$= \phi_0\rho^0_\mathrm{s} + \eta_0\rho^0_\mathrm{f}$	mean density
ρ^0_r	$= \left(1/\phi_0\rho^0_\mathrm{s} + 1/\eta_0\rho^0_\mathrm{f}\right)^{-1}$	reciprocal or reduced density
ρ_{12}	$= -(\mathrm{S}-1)\eta_0\rho^0_\mathrm{f}$	induced mass-coefficient
ρ^0_i	$= \rho^0_\mathrm{r} - \rho_{12} = (\mathrm{S}-\mathrm{m_f})\,\eta_0\rho^0_\mathrm{f}$	modified reciprocal density
$\mathrm{m_s}$	$= \phi_0\rho^0_\mathrm{s}/\rho^0_\mathrm{m}$	solid mass fraction
$\mathrm{m_f}$	$= \eta_0\rho^0_\mathrm{f}/\rho^0_\mathrm{m}$	fluid mass fraction
$\mathrm{m_d}$	$= \eta_0\mathrm{m_s} - \phi_0\mathrm{m_f}$	difference density fraction
	$= \eta_0\phi_0(\rho^0_\mathrm{s} - \rho^0_\mathrm{f})/\rho^0_\mathrm{m}$	alternate form of difference density fraction
	$= \rho^0_\mathrm{r}\left(1/\rho^0_\mathrm{f} - 1/\rho^0_\mathrm{s}\right)$	alternate form of difference density fraction
$\mathrm{d_s}$	$= \phi_0\rho^0_\mathrm{s}/\rho^0_\mathrm{i} = \frac{\mathrm{m_s}}{\mathrm{m_f}}\frac{1}{\mathrm{S}-\mathrm{m_f}}$	solid fraction of modified reciprocal density
$\mathrm{d_f}$	$= \eta_0\rho^0_\mathrm{f}/\rho^0_\mathrm{i} = \frac{1}{\mathrm{S}-\mathrm{m_f}}$	fluid fraction of modified reciprocal density
ν_f	$= \mu_\mathrm{f}/\rho^0_\mathrm{f}$	fluid kinematic shear viscosity
Ω_b	$= \eta_0\nu_\mathrm{f}/K$	Biot critical frequency
Ω_i	$= \mathrm{d_f}\Omega_\mathrm{b}$	Biot relaxation frequency
$\mathrm{K_{fl}}$	$= \eta_0\mathrm{M}^\star$	bulk modulus of pore fluid within deformable frame
H_0	$= \mathrm{K}_0 + \frac{4}{3}\mu_0$	dry-frame P-wave elastic modulus
$\mathrm{H}^\star_\mathrm{c}$	$= \mathrm{H}_0 + \alpha\alpha^\star\mathrm{M}^\star$	generalized Gassmann P-wave elastic modulus
Ω_fP	$=\mathrm{K_f}/(\xi_\mathrm{f} + \frac{4}{3}\mu_\mathrm{f})$	free fluid P-modulus relaxation frequency
Ω_fS	$=\mathrm{K_f}/\mu_\mathrm{f}$	free fluid shear relaxation frequency
Ω_flP	$=\eta_0\mathrm{M}^\star/(\frac{\eta_0\mathrm{M}^\star}{K_\mathrm{f}}\xi_\mathrm{f} + \frac{4}{3}\mu_\mathrm{f})$	pore fluid P-modulus relaxation frequency
Ω_flS	$=\eta_0\mathrm{M}^\star/\mu_\mathrm{f}$	pore fluid shear relaxation frequency
Ω_α	$=\mathrm{H}^\star_\mathrm{c}/(\frac{\eta_0\mathrm{M}^\star}{\mathrm{K_f}}\xi_\mathrm{f} + \frac{4}{3}\mu_\mathrm{f})$	saturated-frame P-modulus relaxation frequency
Ω_β	$=\mu_0/\mu_\mathrm{f} = (\beta^2_c/\nu^\mathrm{f})\eta_0/\mathrm{m^f}$	saturated-frame shear relaxation frequency
α^2_fl	$= \mathrm{K_{fl}}/\rho^0_\mathrm{f}$	vel. of sound within pore-fluid in deform. frame (sqrd)
α^2_s	$= (\mathrm{K_s} + \frac{4}{3}\mu_\mathrm{s})/\rho^0_\mathrm{s}$	mineral P-wave velocity (squared)
β^2_s	$= \mu_\mathrm{s}/\rho^0_\mathrm{s}$	mineral S-wave velocity (squared)
α^2_0	$= \mathrm{H}_0/\phi_0\rho^0_\mathrm{s}$	dry-frame P-wave velocity (squared)
β^2_0	$= \mu_0/\phi_0\rho^0_\mathrm{s}$	dry-frame S-wave velocity(squared)
$\alpha^{\star 2}_\mathrm{c}$	$= \mathrm{H}^\star_\mathrm{c}/\rho^0_\mathrm{m}$	generalized Gassmann P-wave velocity (squared)
β^2_c	$= \mu_0/\rho^0_\mathrm{m}$	Gassmann S-wave velocity(squared)
α^2_I		fast P-wave velocity (squared)
α^2_II		slow P-wave velocity (squared)
β^2_I		fast S-wave velocity (squared)
β^2_II		slow S-wave velocity (squared)

Chapter 1 Introduction

1.1 Background and perspective

Reservoir seismology aims, from the wave field data, to delineate reservoir structure as well as to quantify the type of saturating geo-fluid (whether it is oil, or gas, or water), its volume (i.e., the porosity) and whether it will flow (i.e., the permeability). Reservoirs are elastic matrices saturated with a fluid, that is, porous media. Therefore, the poroelastic theory ought to be the natural framework to analyze waves propagating in reservoirs. It considers the role of fluid phase on equal footing to that of solid phase. Porosity, permeability, and fluid properties are explicitly present in this framework. Apart from the unison motion of phases, this framework takes also into account the relative motion of phases. In contrast, the framework of elasticity is limited only to the motion of phases in unison.

Plona (1980) corroborated experimentally the existence of a slow compressional wave predicted by the poroelasticity theory by Biot (1956, 1962). Slow waves are processes wherein relative motion of the fluid phase with respect to the solid frame dominates. Plona's experiment was a turning point. With that experimental demonstration of relative motion of phases, the framework of poromechanics due to Biot became a viable candidate for seismic wave propagation modeling. However, there is a riddle. In the surface seismic band (2-100 Hz), the predicted attenuation by the Biot theory is orders of magnitude smaller than observed attenuation in field data, although, the predicted velocity is well in agreement.

The Biot theory predicts P- and S- waves, akin to seismic waves predicted by the elasticity theory, which are essentially in-phase motion of the phases. Apart from them, it also predicts an additional process that is of diffusive character up to a cross-over frequency and thereafter propagatory, and it is essentially out of phase compressive motion of the phases.

From a poromechanics point of view, there are two intrinsic mechanisms of attenuation, namely, (a) the relative motion of fluid with respect to solid frame and (b) the viscous relaxation within the fluid itself. Both mechanisms have a pronounced role of the fluid. Thus, from point of view this framework, seismic attenuation is ought to be a key for characterization of geo-fluids. There

have been concerted efforts to understand and quantify the fluid effect on seismic velocity and attenuation by performing laboratory studies.

The pulse transmission technique is the earliest method applied to rocks. In this technique two transducers, a transmitter and a receiver, are attached to the opposite ends of a sample and the propagating signal's travel time and amplitude are measured. The wave attenuation is quantified by the decrement in amplitude of the pulse. By late seventies appropriate compressibility rigs were commissioned at several academic institutions and industrial laboratories to perform pulse propagation experiments under the ambient pressure conditions of reservoir, on sandstones from a variety of geological settings (Toksoz et al., 1979; Winkler, 1983). This method requires that the travel distance for pulse propagation must be at least a few wavelengths long. Since a compressibility rig can accommodate a sample no longer than 10 to 15 cm. The frequency in such experiments is limited to ultrasonic band (0.1-2 MHz). There is a wide agreement in the literature that for sandstones the measured velocity and attenuation in the ultrasonic band corroborate well with the values predicted by the Biot theory (Bourbie et al., 1987; Best et al., 1994), provided the micro-structure is such that equalization of the fluid pressure occurs at pore-scale.

By the end of seventies, the adaptation of resonance bar technique to rocks allowed the extension of the measurements range to the kHz regimen (Winkler and Nur, 1979; Tittmann et al., 1981). In this method, a cylindrical core is excited into extensional mode of vibration. The sample length and elastic properties define the peak resonance frequency. The attenuation is estimated from the decay time of the resonance peak, once the exciting force is removed (Birch and Bancroft, 1938; Born, 1941; Gardner et al., 1964). It is not possible to handle a rock core longer than a meter, which constrains the lower bound of the resonance frequency to the kHz band. For a long time there was a controversy, since the measured extensional attenuation turned out to be higher than the attenuation predicted by the poroelasticity theory. However, by mid-eighties, this was explained by White (1986). By analyzing the poroelastic extensional vibration in the Biot framework (Gardner, 1962), he showed that observed attenuation is due to the boundary effect of the stress-free radial surface of core that allows saturating fluid to freely move in and out.

In the early eighties there was an effort to carryout experimental studies of sub-resonance extensional deformation of cylindrical cores in the low frequency band (sub kHz) utilizing an innovative adaptation of the Hoek apparatus (Spencer, 1981). This is a forced oscillation technique. It studies the dynamic stress-strain relation on a cylindrical sample under a periodic uniaxial stress

that induces low strain ($\sim 10^{-6}$) such that the linear relation holds. This technique excites an extensional mode over the cylinder. From the magnitude of the applied axial stress to measured axial strain the Young modulus is calculated. The phase difference measured between stress and strain signal is used for determining the lossy part of the modulus.

Early experiments on forced oscillation of cylindrical cores were performed around 100Hz with the radial surface of core sample subjected to stress-free condition with the saturating fluid permitted to freely move in and out (Spencer, 1981). Significant attenuation was observed, akin to resonance bar experiment results, and likewise, explained by (Dunn, 1986) as a consequence of boundary effects, caused by the fluid flow through the open-pore stress-free radial surface of the sample.

Based upon his analysis within the framework of quasi-static Biot poroelasticity, with his definition of closed-pore surface (or sealed surface) boundary as unison motion of the solid and fluid phases in normal direction, Dunn (1986) concluded that if a porous cylinder is undergoing unison motion at its exterior surface, it must be under unison motion in its interior as well, thereby, it must behave as an effective ”undrained” solid. Thereafter, Dunn (1987) proposed that, perhaps, by sealing the radial surface with an impermeable coating (of negligible mass) such boundary effect may be eliminated, and presumably, the intrinsic portion of the attenuation for the rock can be measured.

With that, a new era of experimental research in low frequency sub-resonance extensional mode with sealed boundary (LF) began which has been on for the past three decades but without any benefit of a rigorous analytical scrutiny. The experimental community heuristically assumes that in such experiments the sample is an effective elastic solid, no longer an interacting poro-continuum (Batzle et al., 2006). Here the aims have been to develop innovations in apparatus to mimic ambient conditions of reservoir and to bring measurements down to the surface seismic band (2-100 Hz) and even lower to mHz range (Liu and Peselnick, 1983; Jackson et al., 1984, 2011; Batzle et al., 2006; Tisato and Madonna, 2012; Madonna and Tisato, 2013; Subramaniyan et al., 2014; Pimienta et al., 2015; Spencer and Shine, 2016). The overriding concern of experimental low frequency research is to identify the missing intrinsic mechanism(s) that can explain the riddle of underestimation of seismic attenuation by the Biot theory in low seismic band, which otherwise corroborates well with laboratory measurements.

Berryman (1983) has carried out an analysis of the closed-pore case in the Biot framework for the ultrasonic band. He has shown that there are at least two fundamental extensional modes for the closed-pore case. One of them corresponds to the extensional mode wherein phases are in unison motion, and the other extensional mode is close to the slow P-wave in its character.

The closed-pore analysis of Dunn (1986) that lead to ”effective elastic solid” is under the assumption that the sealed surface of the sample is externally open to air, i. e., stress-free with vanishing total stress of the phases in the direction normal to the cylindrical surface. However, in a LF experimental setting the external surface of the sample is in fact jacketed and it is subjected to external pressure to hold the seal. Thus, the observed attenuation in LF experiments is for the case of a boundary that is stressed and sealed, not a boundary that is stress-free and sealed. The latter is a homogeneous boundary condition so it may permit excitation of a pure fundamental mode, the first extensional mode (of the Berryman kind) and the sample may looks like an effective elastic solid. However, the former is an inhomogeneous boundary condition; it will lead to the excitation of all fundamental modes. Since the second extensional mode (of Berryman kind) is diffusive in character, the energy pumped into this mode would dissipate and the sample would appear lossy. These points have escaped the attention of the LF experimentalists.

Furthermore, the analysis of Berryman as well as Dunn are not complete, in the sense that the condition along the tangential direction of the cylindrical surface of the core is unspecified for their sealed boundary problem; they did not make any statement if the two phases in transverse direction are unison or the tangential components of tractions of the two phases are balanced. Also, only the fluid pressure part appears in their analyses. In any case, both shortcomings are due to inherent limitation in the Biot framework, which excludes viscous stress from the very outset (§2.1). At the time of their work an extended Biot framework that included the missing viscous stress term was not available. A generalized framework, called dCS, which includes the missing viscous term came into being by the mid-nineties, for which the Biot framework is a special case (§2.2).

1.2 Thesis objectives and accomplishments

The objective of this work is to develop, based on the dCS theory of poroelasticity, the understanding to interpret the LF attenuation measurements, which are sub-resonance extensional

motions of a sealed porous cylinder subjected to external pressure on its radial surface. It is to investigate if the observed attenuations are due to an intrinsic property because the sample behaves as an effective elastic solid, or it is due to the excitation of additional unknown poroelastic extensional mode(s). To achieve this, the following specific objectives are proposed:

1. Study the natural boundary conditions that are associated with the dCS poroelastic wave equation and, thereby, deduce the impermeable boundary condition.
2. In the dCS framework, establish and solve the dispersion relation for the longitudinal motion of porous cylinder with a stress-free impermeable radial surface.
3. Study the nature of the extensional modes that exist in a saturated porous cylinder with stress-free impermeable radial surface.
4. Develop the asymptotic approximation which relates the velocity and attenuation of the first extensional mode with the material properties.

An overview of the dCS theory is presented in chapter 2 with a succinct description of the governing equations. In chapter 3, the adjoint boundary conditions associated with the dCS poroelastic wave equation are presented. The choice for the impermeable boundary condition is made on the basis of physical reasonings. In chapter 4, the boundary value problem for the longitudinal motion of a fluid-saturated porous cylinder is formulated and the dispersion relation is worked out. Afterwards, in chapter 5, the dispersion relation is specialized for the extensional modes, which is solved numerically by the companion matrix technique (Golub and Van Loan, 1996; Section 7.4.6). The solution shows that there are three natural extensional modes for this case. The nature of these modes is described in chapter 6 and the concluding remarks are presented in chapter 7.

Chapter 2 The poroelastic equations of motion

This chapter presents a brief account of the Biot theory in §2.1, and then introduces the dCS theory. The latter may be viewed as a generalized framework that includes the former as a special case. The Biot constitutive equations have missing viscous stress term and do not include non-reciprocal interaction of compressive stresses of phases. These limitations are accounted for in the dCS constitutive equations, which are presented in §2.2. They are in the form wherein their generalizations over the Biot constitutive equations are apparent. Thereafter, the equations of motion are recast in terms of field variables which are associated with fluxes for mass, momentums and energy of poro-continuum. They are naturally conserved across material discontinuities, and are compatible with recording/ measuring devices. Subsequently, the equations of motion are presented in a compact notation that allows to view them as a 2x2 matrix generalization of the equation of motion of viscoelasticity with Rayleigh dissipation. Finally those are expressed in the frequency domain. For clarity and ease, all field variables and parameters appearing in this chapter are also listed separately in the table of notations.[1]

2.1 The Biot theory

The foremost poroelastic framework of elastic wave propagation was developed by Biot (1956, 1962). From the outset, Biot deals with macroscopic quantities. The averaged displacement fields of solid-frame and saturating fluid are taken as the field quantities. The Biot equations of motion are set up via the Lagrangian approach by using the concepts of elastic energy potential, kinetic energy density function and dissipation function. However, because of its very methodology, the Biot constitutive equations have two major inherent limitations:

(A) Viscous stress is unaccounted: Biot constitutive relations are constructed by the variational approach of “elastic energy potential”, which do not permit the presence of a rate term, since it has to be a conserved quantity. Because the viscous stress part is missing in its (averaged) fluid stress tensor, the bulk and shear viscous-loss mechanisms of pore fluid are not accounted for. As a result, the fluid limit of Biot constitutive relations, obtained by tending porosity to unity, does not converge to the constitutive relation for a Newtonian fluid. Instead,

[1] This chapter is based on lecture notes of CT1652 Física de medios porosos (Personal communications; P. Sahay, 2016).

it is the constitutive relation for an ideal fluid. Furthermore, due to the lack of fluid viscous stresses, the second (or slow) shear process, which accounts for relative shear motions of the two phases, is non-propagating, i.e., it is a process with zero velocity.

The net result is that even though the Biot theory has six translational degrees of freedom, it has to be recast in terms of four degree of freedom for studying a boundary value problem, otherwise a mathematical inconsistency is encountered. However, doing so also completely eliminates relative shear motion of phases from the framework.

(B) Non-reciprocal interactions are unaccounted: Biot's axiomatic definition of the elastic energy potential assumes it to be a single function of 'average solid strain' and 'increase of fluid content'. The 'increase of fluid content' in turn is connected to the 'fluid dilatation strain', that is, the divergence of the average 'fluid displacement field'. Since the energy potential has to be a well-behaved and differentiable function of its arguments, a reciprocity relation follows from the symmetry of its partial derivatives. This symmetry requires a reciprocal interaction of compressive stresses of phases.

As a result of such embedded reciprocity relation in the Biot constitutive equation, the unjacketed bulk and pore-space moduli are expected to be equal. The equality of moduli is also indicative of a macroscopically homogeneous porous material that is also homogeneous at the micro- (pore-) scale (Nur and Byerlee, 1971). However, by now ample experimental evidence exists showing that some rocks exhibit differences in unjacketed bulk and pore-space moduli (Al-Tahini et al., 2005; Hart and Wang, 2010, Blöcher et al., 2014; Pimenta et al., 2017).

Brown and Korringa (1975) have pointed out that a porous material that is macroscopically homogeneous but microscopically inhomogeneous will exhibit unequal unjacketed bulk and pore-space moduli. Apart from them, others, notably Berryman (1992), have attempted to incorporate an additional parameter in the Biot constitutive equations to account for this inequality due to micro-inhomogeneity.

Those attempts of extensions have failed to recognize that the unequal unjacketed bulk and pore-space moduli is indicative of broken symmetry of the reciprocal interaction. Neverthe-

less, the auxiliary equation that mediates the reciprocal interaction is not explicitly stated in the Biot framework. Thus, there are no means to carry-out the extension that incorporates the non-reciprocal interaction of phases to the Biot constitutive equations, unless and until, there is a way to extract-out the (implicit) auxiliary equation of interaction (Sahay, 2013).

2.2 The dCS theory

2.2.1 A generalized framework

The dCS theory of poromechanics has its origin in de la Cruz and Spanos (1985, 1989a, 1989b), de la Cruz et al., (1993), and Hickey et al., (1995), and it is further developed in Sahay et al., (2001) and Sahay (1996, 2001, 2008, 2013). This formulation is based on the mathematics of volume-averaging (Slattery, 1967; Whitaker, 1967; Marle, 1967; Anderson and Jackson, 1967) aided by order-of-magnitude and physical arguments. It obtains macroscopic continuity equations, constitutive relations and equations of motion from the underpinning pore-scale equations. The pore-scale equations exist in the frameworks of well established linear elasticity theory and Naiver-Stokes equation. The links of poroelastic parameters to constituent end-members physical properties are naturally apparent in this framework. The fluid viscous stress term that had to be ruled out from the very outset in the Biot framework, is included here from first principles (i.e. the Navier Stokes Stresses). Also, this framework explicitly takes into account the interfacial strain (i. e., the strain at pore interfaces or pore-deformation strain) that mediates the deformational interactions of phases, which is not apparent in the Biot framework.

The dCS constitutive equations in terms of phasic fields

In the following, for definiteness, a two-phase poro-continuum made up of an elastic solid matrix filled with a chemically inert viscous fluid is considered. It is assumed that there are no sinks or sources of heat, and temperature remains unaltered during deformations so that thermo-mechanical coupling can be ignored. For the case that pores and interfaces are distributed randomly and the two end components are themselves homogeneous and isotropic when unperturbed, the dilatational and deviatoric parts of the pore-deformation strain, respectively, are taken to be affected by the macroscopic pressure of both phases and the macroscopic shear stress of

solid phase (Sahay et al., 2001). With these physical arguments, together with the assumption that the linear elasticity holds true for the porous frame devoid of fluid (Sahay, 2008, Appendix B; Sahay 2013), the sum of strain at pore interfaces, per unit volume of poro-continuum, is given by

$$e^{\star}_{jk} = \phi_0 \frac{\delta_{\mathrm{K}}}{1-\delta_{\mathrm{K}}} \frac{1}{\mathrm{K_s}} \left(\mathrm{p^s} - n\ \mathrm{p^f} \right)\ \delta_{jk} - \frac{\delta_{\mu}}{1-\delta_{\mu}} \frac{1}{2\mu_{\mathrm{s}}} \breve{\tau}^{\mathrm{s}}_{jk}. \tag{1}$$

Here, $\mathrm{p^s}$ and $\mathrm{p^f}$ are the solid and fluid macroscopic pressures, respectively, and $\breve{\tau}^{\mathrm{s}}_{jk}$ is the trace-free part of macroscopic solid stress tensor. $\mathrm{K_s}$ and μ_{s} are the constituent solid bulk and shear moduli, respectively. For convenience, $1-\eta_{_0} \equiv \phi_{_0}$ is introduced. The quadruplet set $\{\eta_0, \delta_{\mathrm{K}}, \delta_{_\mu}, n\}$ are the frame properties, which mediate deformational interactions of phases. They are, respectively, unperturbed porosity, bulk and shear moduli decrement parameters of solid-frame and the measure of non-reciprocal interaction (micro-inhomogeneity). The first three frame parameters are bounded between zero and unity. The micro-inhomogeneity parameter is bounded between zero and $\frac{1}{\delta_{\mathrm{K}}}$, although, its wider upper bound is $\frac{\mathrm{K_s}}{\mathrm{K_f}}$. For $n=1$, equation (1) specialize to the case of reciprocal interaction of compressive stresses of phases.

The constituent solid properties and the frame properties, together with $\{\mathrm{K_f}, \xi_{\mathrm{f}}, \mu_{\mathrm{f}}\}$, namely, the constituent fluid bulk modulus, bulk and shear viscosities, are the 9 parameters of dCS constitutive equations. The host of other poroelastic parameters, which arise in the context of various deformation processes, are a combination of these 9 parameters. For the case of the above auxiliary equation (1) for deformational interactions of phases, the dCS theory yields the solid and fluid macroscopic stresses, respectively, as

$$\tau^{\mathrm{s}}_{jk} \;=\; K_0 \mathrm{u}^{\mathrm{s}}_{ll}\delta_{jk} + 2\mu_0 \breve{\mathrm{u}}^{\mathrm{s}}_{jk} - n\ \left(\alpha - \eta_{_0}\right) \mathrm{p^f}\delta_{jk}, \tag{2}$$

and

$$\tau^{\mathrm{f}}_{jk} \;=\; -\eta_{_0}\mathrm{p^f}\delta_{jk} \underline{- \eta_{_0} \frac{\xi_{\mathrm{f}}}{K_{\mathrm{f}}} \frac{\partial \mathrm{p^f}}{\partial t}\delta_{jk} + 2\mu_{\mathrm{f}} \left\{ \eta_{_0} \frac{\partial \breve{\mathrm{u}}^{\mathrm{f}}_{jk}}{\partial t} + \phi_{_0}\delta_{_\mu} \frac{\partial \breve{\mathrm{u}}^{\mathrm{s}}_{jk}}{\partial t} \right\}} \tag{3}$$

with the macroscopic pressure given by

$$\mathrm{p^f} \;=\; -\mathrm{M}^{\star} \left(\alpha \mathrm{u}^{\mathrm{s}}_{ll} - \zeta \right). \tag{4}$$

The above equations are expressed in the form akin to Biot (1962) for the ease of their direct comparison with the Biot constitutive equations. Here, $\mathrm{u}^{\mathrm{s}}_{jk}$ and $\mathrm{u}^{\mathrm{f}}_{jk}$ are, respectively, the solid and fluid macroscopic strain tensors and their trace-free parts are $\breve{\mathrm{u}}^{\mathrm{s}}_{jk}$ and $\breve{\mathrm{u}}^{\mathrm{f}}_{jk}$. $\zeta = -\eta_{_0}\left(\mathrm{u}^{\mathrm{f}}_{ll} - \mathrm{u}^{\mathrm{s}}_{ll}\right)$ is interpreted as the increase of fluid content. The quintet set $\{\mathrm{K}_{_0}, \mu_{_0}, \alpha, \alpha^\star, \mathrm{M}^\star\}$ are the derived parameters $\phi_0(1-\delta_{\mathrm{K}})\mathrm{K}_{\mathrm{s}} \equiv \mathrm{K}_{_0}$, $\phi_0(1-\delta_{\mu_s})\mu_{\mathrm{s}} \equiv \mu_{_0}$, $\eta_{_0} + \phi_0\delta_{\mathrm{K}} \equiv \alpha$, $\eta_{_0} + \phi_0\delta_{\mathrm{K}}\, n \equiv \alpha^\star$ and $\frac{\eta_0}{K_{\mathrm{f}}} + n\frac{\eta_0\delta_{\mathrm{K}}}{K_{\mathrm{s}}} \equiv \frac{1}{\mathrm{M}^\star}$. They are identified as solid-frame bulk and shear moduli, the Biot bulk coefficient, the effective pressure coefficient for bulk volume and the generalized fluid storage coefficient. They are the typical geomechanical parameters, which are measured by compressibility experiments. The underlined term in (3) is the macroscopic fluid viscous stress term omitted in the Biot framework. In equations (2)-(4), by dropping this term and setting micro-inhomogeneity parameter $n = 1$, the dCS constitutive equations specialize to the Biot constitutive equations.

Substituting equation (4) into equations (2) and (3), and expressing the macroscopic fluid pressure term therein in terms of the solid and fluid volumetric strains, the dCS constitutive equations are cast as

$$\begin{pmatrix} \tau^{\mathrm{s}}_{jk} \\ \tau^{\mathrm{f}}_{jk} \end{pmatrix} = \left(\mathbf{K}_{\mathrm{b}} + \boldsymbol{\xi}_{\mathrm{b}}\partial_t\right)\begin{pmatrix} \mathrm{u}^{\mathrm{s}}_{ll} \\ \mathrm{u}^{\mathrm{f}}_{ll} \end{pmatrix}\delta_{jk} + 2\left(\boldsymbol{\mu}_{\mathrm{b}} + \boldsymbol{\nu}_{\mathrm{b}}\partial_t\right)\begin{pmatrix} \breve{\mathrm{u}}^{\mathrm{s}}_{jk} \\ \breve{\mathrm{u}}^{\mathrm{f}}_{jk} \end{pmatrix}, \tag{5}$$

where the following definitions have been employed

$$\begin{pmatrix} K_0 + \left(\alpha - \eta_{_0}\right)\left(\alpha^\star - \eta_{_0}\right)\mathrm{M}^\star & (\alpha-\eta_{_0})\eta_{_0}\mathrm{M}^\star \\ (\alpha-\eta_{_0})\eta_{_0}\mathrm{M}^\star & \eta_0^2\mathrm{M}^\star \end{pmatrix} \equiv \mathbf{K}_{\mathrm{b}}, \tag{6}$$

$$\begin{pmatrix} 1 & 0 \\ 0 & 0 \end{pmatrix}\mu_0 \equiv \boldsymbol{\mu}_{\mathrm{b}}. \tag{7}$$

$$\begin{pmatrix} 0 & 0 \\ \phi_{_0}\delta_{_{\mathrm{K}}} & \eta_{_0} \end{pmatrix}\frac{\eta_0\mathrm{M}^\star}{K_{\mathrm{f}}}\xi_{\mathrm{f}} \equiv \boldsymbol{\xi}_{\mathrm{b}}, \tag{8}$$

and

$$\begin{pmatrix} 0 & 0 \\ \phi_0\delta_\mu & \eta_0 \end{pmatrix} \mu_{\mathrm{f}} \equiv \boldsymbol{\nu}_{\mathrm{b}}. \tag{9}$$

$\boldsymbol{K}_{\mathrm{b}}$ and $\boldsymbol{\mu}_{\mathrm{b}}$ are viewed as the bulk- and shear- modulus elastic coefficient matrices. $\boldsymbol{\xi}_{\mathrm{b}}$ and $\boldsymbol{\nu}_{\mathrm{b}}$ are the bulk and shear viscosity matrices. By setting the bulk and shear viscosities vanishing, the matrices incorporating fluid viscous relaxation processes, $\boldsymbol{\xi}_{\mathrm{b}}$ and $\boldsymbol{\nu}_{\mathrm{b}}$, are dropped and the Biot constitutive equations are recovered, once the micro-inhomogeneity parameter n is also set to unity. The incorporation of fluid viscous relaxation terms render the form of this constitutive relation to be a 2×2 matrix generalization of viscoelastic constitutive relation.

The dCS equations of motion in terms of phasic fields

In the dCS framework the two vector fields that describe the trajectories of the solid and fluid masses are defined through their respective macroscopic continuity equation. That ensures these fields are associated with the conservation of the solid and fluid mass at macro-scale, as it should be. The equations of motion, expressed in terms of average solid and fluid displacements, read

$$\phi_0\rho_{\mathrm{s}}^{\circ}\frac{\partial^2 \mathrm{u}_j^{\mathrm{s}}}{\partial t^2} = \tau_{jk,k}^{\mathrm{s}} + \mathrm{I}_j \tag{10}$$

$$\eta_0\rho_{\mathrm{f}}^{\circ}\frac{\partial^2 \mathrm{u}_j^{\mathrm{f}}}{\partial t^2} = \tau_{jk,k}^{\mathrm{f}} - \mathrm{I}_j \tag{11}$$

where $\rho_{\mathrm{s}}^{\circ}$ and $\rho_{\mathrm{f}}^{\circ}$ are the unperturbed solid and fluid densities, respectively. As phases deform not only they induce deformational forces (stresses) within themselves, they also exert forces (intercomponent-interaction forces) on each other. Since Newton's third law must hold true, the intercomponent-interaction forces must be equal and opposite. In dCS framework this internal force is quantified as the sum of forces exerted by one phase on the other through pore-interfaces in a unit volume of the porous medium, and it appears as an effective body force, I_j, in the equations of motion. Guided by the dissipative function and kinetic energy density function as developed in the Biot framework, it is taken as

$$\mathrm{I}_j = \eta_0 \rho_{\mathrm{f}}^{\circ} \Omega_{\mathrm{b}} \frac{\partial}{\partial t} \left(\mathrm{u}_j^{\mathrm{f}} - \mathrm{u}_j^{\mathrm{s}} \right) - \rho_{12} \frac{\partial^2}{\partial t^2} \left(\mathrm{u}_j^{\mathrm{f}} - \mathrm{u}_j^{\mathrm{s}} \right) \tag{12}$$

where $\Omega_{\mathrm{b}} = \eta_0 \nu_{\mathrm{f}} / \kappa$ is the Biot critical frequency, $\nu_{\mathrm{f}} = \mu_{\mathrm{f}} / \rho_{\mathrm{f}}^{\circ}$ is the pore-fluid kinematic shear viscosity and κ is the permeability. ρ_{12} is the induced mass coefficient which is linked to tortuosity, S, as $\rho_{12} = -(S-1)\eta_0 \rho_{\mathrm{f}}^{\circ}$.

For clarity, the equations of motion (10 and 11) recast as

$$\begin{pmatrix} \phi_0 \rho_{\mathrm{s}}^{\circ} & 0 \\ 0 & \eta_0 \rho_{\mathrm{f}}^{\circ} \end{pmatrix} \partial_t^2 \begin{pmatrix} \mathrm{u}_j^{\mathrm{s}} \\ \mathrm{u}_j^{\mathrm{f}} \end{pmatrix} = \begin{pmatrix} \tau_{jk,k}^{\mathrm{s}} \\ \tau_{jk,k}^{\mathrm{f}} \end{pmatrix} + \begin{pmatrix} 1 \\ -1 \end{pmatrix} \mathrm{I}_j \tag{13}$$

and substituting in the above the expression of I_j from equation (12) results in

$$\begin{pmatrix} \phi_0 \rho_{\mathrm{s}}^{\circ} - \rho_{12} & \rho_{12} \\ \rho_{12} & \eta_0 \rho_{\mathrm{f}}^{\circ} - \rho_{12} \end{pmatrix} \partial_t^2 \begin{pmatrix} \mathrm{u}_j^{\mathrm{s}} \\ \mathrm{u}_j^{\mathrm{f}} \end{pmatrix} + \eta_0 \rho_{\mathrm{f}}^{\circ} \Omega_{\mathrm{b}} \begin{pmatrix} 1 & -1 \\ -1 & 1 \end{pmatrix} \partial_t \begin{pmatrix} \mathrm{u}_j^{\mathrm{s}} \\ \mathrm{u}_j^{\mathrm{f}} \end{pmatrix} = \begin{pmatrix} \tau_{jk,k}^{\mathrm{s}} \\ \tau_{jk,k}^{\mathrm{f}} \end{pmatrix}. \tag{14}$$

2.2.2 The dCS framework of centre-of-mass and internal fields: The natural fields

Surface measurements of wave motions consist of the three components of the displacement. The phasic formulation of poroelasticity uses two displacement fields to describe the motion of the solid-frame and the saturating fluid. Within this formulation of poroelasticity, there is no compatible map between these six displacement components to the three components of displacement recorded at the material surface.

To resolve this, Sahay (1996) interpreted poroelasticity as a two-body problem. He suggested that the natural fields for dynamical problems are the centre-of-mass (mean) field and internal (rotational) field. The former is the mass fraction weighted vector sum of solid and fluid phasic fields. The latter is the difference density fraction weighted vector difference of solid and fluid phasic fields.

In terms of new dynamical fields the equations of balance of mass, momentums and energy

for porous media take the same form as the single continuum statements. The total mass of poro-continuum is conserved with centre-of-mass field and it is associated with total linear momentum flux. It describes the transport of translational kinetic energy, therefore, it represents three translational degrees of freedom of material points. The Internal field is associated with spin (angular momentum about centre-of-mass) flux. It describes transport of rotational kinetic energy, therefore, it represents three rotational degrees of freedom of material points. Since current recording devices register translational degrees of freedom and measures the field associated with total linear momentum, they indeed track centre-of-mass field.

The centre-mass or mean field is defined as

$$\mathrm{u}_j^{\mathrm{m}} \quad = \quad m_s \mathrm{u}_j^{\mathrm{s}} + m_f \mathrm{u}_j^{\mathrm{f}}, \tag{15}$$

where $m_s = \frac{\phi_0 \rho_s^0}{\rho_m^0}$ and $m_f = \frac{\eta_0 \rho_f^0}{\rho_m^0}$ are solid and fluid mass fractions, respectively, and $\rho_m^0 = \phi_0 \rho_s^0 + \eta_0 \rho_f^0$ is the mean or total density of poro-continuum. The deformational force that drives this field is associated with the total or mean stress of poro-continuum, given by

$$\tau_{jk}^{\mathrm{m}} \quad = \quad \tau_{jk}^{\mathrm{s}} + \tau_{jk}^{\mathrm{f}}. \tag{16}$$

The internal rotational field, which describes a relative motion of the fluid with respect to the solid, can not be measured directly by the current devices. However, it has a pronounced effect on attenuation of center-of-mass field, the field that is recorded by the current devices. The internal field is described by

$$\mathrm{u}_j^{\mathrm{i}} \quad = \quad m_{\mathrm{d}} \left(\mathrm{u}_j^{\mathrm{f}} - \mathrm{u}_j^{\mathrm{s}} \right), \tag{17}$$

where $m_{\mathrm{d}} = \eta_{_0} m_{\mathrm{s}} - \phi_{_0} m_{\mathrm{f}}$ is the difference density fraction. This dimensionless difference density fraction term ensures that in the limit when the elastic properties of the two phases are the same, the force driving the difference motion is the same as the force driving the net motion of the two

phases (Sahay, 2010). The couple-stress that drives this field is given by

$$\tau^{\mathrm{i}}_{jk} \;=\; \frac{1}{m_{\mathrm{d}}}\left(m_{\mathrm{s}}\tau^{\mathrm{f}}_{jk} - m_{\mathrm{f}}\tau^{\mathrm{s}}_{jk}\right). \tag{18}$$

This is called the internal stress of poro-continuum.

Orthogonal transformation matrix

For convenience, an orthogonal transformation matrix is introduced that allows to cast the dCS phasic field framework to natural field framework with an ease. The state variables are defined by

$$\left(\mathrm{u}^{\mathrm{m}}_{j}\;\; \mathrm{u}^{\mathrm{i}}_{j}\right)^{\mathrm{T}} \;=\; \mathbf{T}^{-1}\left(\mathrm{u}^{\mathrm{s}}_{j}\;\; \mathrm{u}^{\mathrm{f}}_{j}\right)^{\mathrm{T}}, \tag{19}$$

in conjunction with its conjugate stresses given by

$$\left(\tau^{\mathrm{m}}_{jk}\;\; \tau^{\mathrm{i}}_{jk}\right)^{\mathrm{T}} \;=\; \mathbf{T}^{\mathrm{T}}\left(\tau^{\mathrm{s}}_{jk}\;\; \tau^{\mathrm{f}}_{jk}\right)^{\mathrm{T}}, \tag{20}$$

where $^{\mathrm{T}}$ stands for transpose. The transformation matrix is defined by

$$\mathbf{T} \;=\; \begin{pmatrix} 1 & -\frac{\mathrm{m_f}}{\mathrm{m_d}} \\ 1 & \frac{\mathrm{m_s}}{\mathrm{m_d}} \end{pmatrix} \tag{21}$$

which gives

$$\mathbf{T}^{\mathrm{T}} = \begin{pmatrix} 1 & 1 \\ -\frac{\mathrm{m_f}}{\mathrm{m_d}} & \frac{\mathrm{m_s}}{\mathrm{m_d}} \end{pmatrix} \quad \text{and} \quad \mathbf{T}^{-1} = \begin{pmatrix} \mathrm{m_s} & \mathrm{m_f} \\ -\mathrm{m_d} & \mathrm{m_d} \end{pmatrix}, \;\; \text{with} \;\; \left(\mathbf{T}^{\mathrm{T}}\right)^{-1} = (\mathbf{T}^{-1})^{\mathrm{T}}. \tag{22}$$

This transformation preserves the strain energy, which is apparent by below

$$\left(\mathrm{u}^{\mathrm{s}}_{jk}\;\; \mathrm{u}^{\mathrm{f}}_{jk}\right)\left(\tau^{\mathrm{s}}_{jk}\;\; \tau^{\mathrm{f}}_{jk}\right)^{\mathrm{T}} = \left(\mathbf{T}(\mathrm{u}^{\mathrm{m}}_{jk}\;\; \mathrm{u}^{\mathrm{i}}_{jk})^{\mathrm{T}}\right)^{\mathrm{T}}\left(\mathbf{T}^{\mathrm{T}}\right)^{-1}\left(\tau^{\mathrm{m}}_{jk}\;\; \tau^{\mathrm{i}}_{jk}\right)^{\mathrm{T}} = \left(\mathrm{u}^{\mathrm{m}}_{jk}\;\; \mathrm{u}^{\mathrm{i}}_{jk}\right)\left(\tau^{\mathrm{m}}_{jk}\;\; \tau^{\mathrm{i}}_{jk}\right)^{\mathrm{T}}. \tag{23}$$

The dCS constitutive equations in terms of natural dynamical fields

Using transformation (20) into equation (5), the dCS constitutive equations are recast in terms of natural dynamical fields as

$$\begin{pmatrix} \tau^{\mathrm{m}}_{jk} \\ \tau^{\mathrm{i}}_{jk} \end{pmatrix} = (\mathbf{K} + \boldsymbol{\xi}\partial_t) \begin{pmatrix} \mathrm{u}^{\mathrm{m}}_{ll} \\ \mathrm{u}^{\mathrm{i}}_{ll} \end{pmatrix} \delta_{jk} + 2\,(\boldsymbol{\mu} + \boldsymbol{\nu}\partial_t) \begin{pmatrix} \breve{\mathrm{u}}^{\mathrm{m}}_{jk} \\ \breve{\mathrm{u}}^{\mathrm{i}}_{jk} \end{pmatrix}, \tag{24}$$

where

$$\mathbf{T}^{\mathrm{T}}\mathbf{K}_{\mathrm{b}}\mathbf{T} \equiv \mathbf{K},\ \mathbf{T}^{\mathrm{T}}\boldsymbol{\xi}_{\mathrm{b}}\mathbf{T} \equiv \boldsymbol{\xi},\ \mathbf{T}^{\mathrm{T}}\boldsymbol{\mu}_{\mathrm{b}}\mathbf{T} \equiv \boldsymbol{\mu},\ \text{and}\ \mathbf{T}^{\mathrm{T}}\boldsymbol{\nu}_{\mathrm{b}}\mathbf{T} \equiv \boldsymbol{\nu}. \tag{25}$$

The dCS equations of motion in terms of natural dynamical fields

Using transformations (19) and (20), the dCS equations of motion (14) are recast in terms of natural dynamical fields as

$$\begin{pmatrix} \rho^{\circ}_{\mathrm{m}} & 0 \\ 0 & \frac{\rho^{\circ}_{\mathrm{i}}}{\mathrm{m}^2_{\mathrm{d}}} \end{pmatrix} \partial_t^2 \begin{pmatrix} \mathrm{u}^{\mathrm{m}}_j \\ \mathrm{u}^{\mathrm{i}}_j \end{pmatrix} + \eta_0 \rho^{\circ}_{\mathrm{f}} \Omega_{\mathrm{b}} \frac{1}{\mathrm{m}^2_{\mathrm{d}}} \begin{pmatrix} 0 & 0 \\ 0 & 1 \end{pmatrix} \partial_t \begin{pmatrix} \mathrm{u}^{\mathrm{m}}_j \\ \mathrm{u}^{\mathrm{i}}_j \end{pmatrix} = \begin{pmatrix} \tau^{\mathrm{m}}_{jk,k} \\ \tau^{\mathrm{i}}_{jk,k} \end{pmatrix}, \tag{26}$$

or,

$$\begin{pmatrix} 1 & 0 \\ 0 & 1 \end{pmatrix} \partial_t^2 \begin{pmatrix} \mathrm{u}^{\mathrm{m}}_j \\ \mathrm{u}^{\mathrm{i}}_j \end{pmatrix} + \underbrace{\frac{\eta_0 \rho^{\circ}_{\mathrm{f}}}{\rho^{\circ}_{\mathrm{i}}} \Omega_{\mathrm{b}}}_{\Omega_{\mathrm{i}}} \begin{pmatrix} 0 & 0 \\ 0 & 1 \end{pmatrix} \partial_t \begin{pmatrix} \mathrm{u}^{\mathrm{m}}_j \\ \mathrm{u}^{\mathrm{i}}_j \end{pmatrix} = \begin{pmatrix} \frac{1}{\rho^{\circ}_{\mathrm{m}}} & 0 \\ 0 & \frac{\mathrm{m}^2_{\mathrm{d}}}{\rho^{\circ}_{\mathrm{i}}} \end{pmatrix} \begin{pmatrix} \tau^{\mathrm{m}}_{jk,k} \\ \tau^{\mathrm{i}}_{jk,k} \end{pmatrix}. \tag{27}$$

Herein, the definition $\rho^{\circ}_{\mathrm{r}} - \rho_{12} \equiv \rho^{\circ}_{\mathrm{i}}$ is also introduced.

2.2.3 Extended dynamical variables framework

For an ease for pursuing analytical work the following notation is introduced

$$\mathbf{u}_j = \begin{pmatrix} \mathrm{u}^{\mathrm{m}}_j & \mathrm{u}^{\mathrm{i}}_j \end{pmatrix}^{\mathrm{T}}, \tag{28}$$

and

$$\boldsymbol{\tau}_{jk} = \left(\tau^{\mathrm{m}}_{jk} \;\; \tau^{\mathrm{i}}_{jk}\right)^{\mathrm{T}}, \tag{29}$$

the preceding equations of motion (26) are rewritten in a compact form as

$$\boldsymbol{\rho}\, \partial_t^2 \mathbf{u}_j + \Omega_{\mathrm{i}} \frac{\rho^{\circ}_{\mathrm{i}}}{\mathrm{m}^2_{\mathrm{d}}}\, \mathbf{I}_0\, \partial_t \mathbf{u}_j = \boldsymbol{\tau}_{jk,k}\,, \tag{30}$$

where $\boldsymbol{\rho}$ is the density matrix

$$\boldsymbol{\rho} \;\; = \;\; \begin{pmatrix} \rho^{\circ}_{\mathrm{m}} & 0 \\ 0 & \frac{\rho^{\circ}_{\mathrm{i}}}{\mathrm{m}^2_{\mathrm{d}}} \end{pmatrix}, \tag{31}$$

and $\frac{\eta_0 \rho^{\circ}_{\mathrm{f}}}{\rho^{\circ}_{\mathrm{i}}} \equiv d_{\mathrm{f}}$ (also $\frac{\phi_0 \rho^{\circ}_{\mathrm{s}}}{\rho^{\circ}_{\mathrm{i}}} \equiv d_{\mathrm{s}}$), and $d_{\mathrm{f}}\Omega_{\mathrm{b}} \equiv \Omega_{\mathrm{i}}$ is the cross-over frequency from viscous to inertial transition (the Biot relaxation frequency), which causes frictional loss. The frictional loss term in a wave-equation is also known as Rayleigh dissipation. $\mathbf{I}_0$ is a 2×2 matrix whose element (2,2) is unity and the rest of the elements are equal to zero, that is,

$$\mathbf{I}_0 \;\; = \;\; \begin{pmatrix} 0 & 0 \\ 0 & 1 \end{pmatrix}. \tag{32}$$

The constitutive equations (24) are re-expressed as

$$\boldsymbol{\tau}_{jk} \;\; = \;\; \left(\mathbf{K} + \boldsymbol{\xi}\partial_t\right) \mathbf{u}_{ll}\delta_{jk} + 2\left(\boldsymbol{\mu} + \boldsymbol{\nu}\partial_t\right) \breve{\mathbf{u}}_{jk}. \tag{33}$$

Notationally, the equations of motion (30) and the constitutive relation (33) are akin to the elasticity theory, however, density and elastic parameters are now 2×2 matrices. Substituting equation (33) into equation (30), and introducing the "extended dynamical vector" $\mathbf{u}$ whose elements are the centre-of-mass and internal rotational field vectors,

$$\mathbf{u} = \hat{\mathbf{e}}_j \mathbf{u}_j = \hat{\mathbf{e}}_j (\mathrm{u}^{\mathrm{m}}_j \;\; \mathrm{u}^{\mathrm{i}}_j)^{\mathrm{T}}, \tag{34}$$

$\hat{\mathbf{e}}_j$ is the unit vector in jth direction, and applying $\boldsymbol{\rho}^{-1}$ from the left, the equations of motion (30) cast in vectorial notation read

$$\mathbf{I}\partial_t^2\mathbf{u} + \Omega_{\mathrm{i}}\mathbf{I}_0\partial_t\mathbf{u} = \boldsymbol{\rho}^{-1}\,\boldsymbol{\tau}_{jk,k}\ , \tag{35}$$

and substituting constitutive equations (33) results in

$$\mathbf{I}\partial_t^2\mathbf{u} + \Omega_{\mathrm{i}}\mathbf{I}_0\partial_t\mathbf{u} = (\mathbf{C}_\alpha + \mathbf{N}_\alpha\partial_t)\,\nabla\,(\nabla\cdot\mathbf{u}) - \left(\mathbf{C}_\beta + \mathbf{N}_\beta\partial_t\right)\nabla\times\nabla\times\mathbf{u}, \tag{36}$$

where $\mathbf{I}$ is the 2×2 identity matrix, and

$$\boldsymbol{\rho}^{-1}\left(\mathbf{K} + \frac{4}{3}\boldsymbol{\mu}\right) \equiv \mathbf{C}_\alpha, \tag{37}$$

$$\boldsymbol{\rho}^{-1}\left(\boldsymbol{\xi} + \frac{4}{3}\boldsymbol{\nu}\right) \equiv \mathbf{N}_\alpha, \tag{38}$$

$$\boldsymbol{\rho}^{-1}\boldsymbol{\mu} \equiv \mathbf{C}_\beta, \tag{39}$$

$$\boldsymbol{\rho}^{-1}\boldsymbol{\nu} \equiv \mathbf{N}_\beta. \tag{40}$$

It is apparent from equation (36) that $\mathbf{C}_\alpha$ and $\mathbf{N}_\alpha$ are associated with compressional processes, whereas $\mathbf{C}_\beta$ and $\mathbf{N}_\beta$ are associated with shear processes. The elements of the second-order $\mathbf{C}_\alpha$ and $\mathbf{C}_\beta$ matrices have dimensions of velocity squared. The elements of the second-order $\mathbf{N}_\alpha$ and $\mathbf{N}_\beta$ matrices have dimensions of kinematic viscosity. It should be noted that these four matrices are real. The explicit expressions of these are

$$\mathbf{C}_{\alpha} = \alpha_{\mathrm{c}}^{\star 2} \begin{pmatrix} 1 & -\frac{1}{\mathrm{m_d}}\mathrm{m_f} \times \left(1 - \frac{\alpha^{\star}}{\eta_0}\frac{\alpha_{\mathrm{fl}}^{\star 2}}{\alpha_{\mathrm{c}}^{\star 2}}\right) \\ -\mathrm{m_d d_f}\left(1 - \frac{\alpha}{\eta_0}\frac{\alpha_{\mathrm{fl}}^{\star 2}}{\alpha_{\mathrm{c}}^{\star 2}}\right) & \mathrm{d_f}\left(\mathrm{m_f} + \varepsilon\right) \end{pmatrix} \tag{41}$$

$$\mathbf{N}_{\alpha} = \alpha_{\mathrm{c}}^{\star 2} \begin{pmatrix} \Upsilon & \frac{1}{\mathrm{m_d}}\left(\eta_0 - \mathrm{m_f}\Upsilon\right) \\ \mathrm{m_d d_s}\Upsilon & d_{\mathrm{s}}\left(\eta_0 - \mathrm{m_f}\Upsilon\right) \end{pmatrix} \frac{1}{\Omega_{\alpha}} \tag{42}$$

$$\mathbf{C}_{\beta} = \beta_{\mathrm{c}}^{2} \begin{pmatrix} 1 & -\frac{\mathrm{m_f}}{\mathrm{m_d}} \\ -\mathrm{d_f m_d} & \mathrm{d_f m_f} \end{pmatrix} \tag{43}$$

$$\mathbf{N}_{\beta} = \beta_{\mathrm{c}}^{2} \begin{pmatrix} \alpha_{\mu} & \frac{1}{\mathrm{m_d}}\left(\eta_0 - \alpha_{\mu}\,\mathrm{m_f}\right) \\ \mathrm{m_d}\alpha_{\mu}\,\mathrm{d_s} & \left(\eta_0 - \alpha_{\mu}\,\mathrm{m_f}\right)\mathrm{d_s} \end{pmatrix} \frac{1}{\Omega_{\beta}}. \tag{44}$$

For an ease in mathematical analysis, the velocity (square) and relaxation frequency terms in (41)-(44) are factorized such that each elements are bounded by unity. $\alpha_{\mathrm{c}}^{\star 2} = \frac{\mathrm{H_c^{\star}}}{\rho_{\mathrm{m}}^{\circ}}$, $\beta_{\mathrm{c}}^{2} = \frac{\mu_0}{\rho_{\mathrm{m}}^{\circ}}$ are (generalized) Gassmann P- and S- wave speed (squared), respectively. Here, $\mathrm{H_c^{\star}} = K_0 + \alpha\,\alpha^{\star}M^{\star} + \frac{4}{3}\mu_0$, is the generalized Gassmann P-wave elastic modulus.

$\Omega_{\alpha} = \frac{\mathrm{H_c^{\star}}}{\frac{\eta_0 \mathrm{M}^{\star}}{K_{\mathrm{f}}}\xi_{\mathrm{f}} + \frac{4}{3}\mu_{\mathrm{f}}}$ and $\Omega_{\beta} = \frac{\mu_0}{\mu_{\mathrm{f}}}$ are the saturated-bulk relaxation frequencies for P- and S-process, respectively. These frequencies are associated with the relaxation of poro-continuum as a whole on account of the relaxation within the pore-fluid.

The term $\varepsilon = \left\{1 - (\alpha + \alpha^{\star})\frac{\mathrm{m_f}}{\eta_0}\right\}\frac{{\alpha_{\mathrm{fl}}}^2}{\alpha_{\mathrm{c}}^{\star 2}}$ is a positive quantity less than unity, and the term $\Upsilon = \alpha + (\alpha_{\mu} - \alpha)\frac{4}{3}\frac{\Omega_{\mathrm{flP}}}{\Omega_{\mathrm{flS}}}$ is bounded as $\alpha \leq \Upsilon \leq \alpha_{\mu}$. ${\alpha_{\mathrm{fl}}}^2 = \frac{\eta_0 \mathrm{M}^{\star}}{\rho_{\mathrm{f}}}$, is identified as the velocity (squared) of sound in fluid in the presence deformable solid-frame. $\Omega_{\mathrm{flP}} = \frac{\eta_0 \mathrm{M}^{\star}}{\frac{\eta_0 \mathrm{M}^{\star}}{K_{\mathrm{f}}}\xi_{\mathrm{f}} + \frac{4}{3}\mu_{\mathrm{f}}}$, $\Omega_{\mathrm{flS}} = \frac{\eta_0 \mathrm{M}^{\star}}{\mu_{\mathrm{f}}}$ are identified as, respectively, fluid P-modulus and fluid S-modulus relaxation frequencies, which are pore-fluid viscous relaxations in the presence of deformable solid-frame.

2.2.4 Frequency domain representation

For the solutions harmonic in time,

$$\mathbf{u}(\mathbf{x},t) = e^{-i\omega t}\,\mathbf{u}(\mathbf{x},\omega), \tag{45}$$

equation (35) reads in frequency domain as

$$\boldsymbol{\Omega}^{-1}\boldsymbol{\rho}^{-1}\,\boldsymbol{\tau}_{jk,k} + \omega^2\mathbf{u} = 0 \tag{46}$$

and its displacement field form (36) is

$$\boldsymbol{\alpha}\nabla\left(\nabla\cdot\mathbf{u}\right) - \boldsymbol{\beta}\nabla\times\nabla\times\mathbf{u} + \omega^2\mathbf{u} \;=\; 0 \tag{47}$$

where $\boldsymbol{\alpha}$ and $\boldsymbol{\beta}$ are the non-symmetric second-order matrices associated with P- and S- motion, respectively, whose elements are dimensionally equal to velocity squared. They are

$$\boldsymbol{\alpha} \;= \boldsymbol{\Omega}^{-1}\left(\mathbf{C}_\alpha - i\omega\mathbf{N}_\alpha\right) \;\equiv \begin{pmatrix} \alpha_{\mathrm{mm}} & \alpha_{\mathrm{mi}} \\ \alpha_{\mathrm{im}} & \alpha_{\mathrm{ii}} \end{pmatrix}, \tag{48}$$

$$\boldsymbol{\beta} \;= \boldsymbol{\Omega}^{-1}\left(\mathbf{C}_\beta - i\omega\mathbf{N}_\beta\right) \;\equiv \begin{pmatrix} \beta_{\mathrm{mm}} & \beta_{\mathrm{mi}} \\ \beta_{\mathrm{im}} & \beta_{\mathrm{ii}} \end{pmatrix}, \tag{49}$$

where $\boldsymbol{\Omega}$ is a 2×2 diagonal matrix associated with the Biot relaxation frequency Ω_{i}.

$$\mathbf{I} + i\,\frac{\Omega_{\mathrm{i}}}{\omega}\,\mathbf{I}_0 \;\equiv\; \boldsymbol{\Omega} \tag{50}$$

where $\mathbf{I}$ is the 2×2 identity matrix and $\mathbf{I}_0$ is the diagonal matrix diag$(0,1)$ defined earlier in (32). This matrix is associated with the Biot relaxation frequency, the cross-over frequency of viscous / inertial transition, and might be named the Rayleigh damping matrix.

Substituting the definitions (37)-(40) into equation (33), the resulting expression for stresses read as

$$\boldsymbol{\tau}_{jk} \;=\; \boldsymbol{\rho}\left[\left\{\left(\mathbf{C}_{\alpha}-i\omega\mathbf{N}_{\alpha}\right)-2\left(\mathbf{C}_{\beta}-i\omega\mathbf{N}_{\beta}\right)\right\}\mathrm{u}_{ll}\delta_{jk}+2\left(\mathbf{C}_{\beta}-i\omega\mathbf{N}_{\beta}\right)\breve{\mathrm{u}}_{jk}\right],$$

which in the view of definitions (48)-(49) are expressed as

$$\boldsymbol{\tau}_{jk} \;=\; \boldsymbol{\Omega\rho}\left\{\left(\boldsymbol{\alpha}-2\boldsymbol{\beta}\right)\mathrm{u}_{ll}\delta_{jk}+2\boldsymbol{\beta}\,\breve{\mathrm{u}}_{jk}\right\}. \tag{51}$$

Chapter 3 Boundary conditions at a stress-free impermeable surface

The poroelastic seismic boundary conditions for an impermeable surface are not properly specified in literature. That is due the inherent limitation of the Biot theory on account of its two redundant degrees of freedom. An overview of the status of the boundary conditions for an impermeable surface, in the framework of Biot theory, is presented in §3.1. Thereafter, in §3.2 the boundary conditions are viewed from the perspective of the dCS framework, the generalized framework that includes the Biot theory as a special case. The set of sixteen natural boundary conditions are deduced that allow the dCS equations of motion to be adjoint. From that set, in §3.3, one finds two natural choices for the boundary conditions for an impermeable surface. Both cases have the motions of two phases in unison at the interface in the direction normal to the interface. However, in direction tangential to the interface, in one case motions of both phases are also in unison, whereas in the other case, stresses of the two phases are balanced at the interface. From physical reasonings, in this work, it is the latter that is taken as the set of boundary conditions for impermeable surface.

3.1 Perspective from literature

The poroelastic seismic boundary conditions are an open research problem. These were first analyzed by Deresiewicz and Skalak (1963) in the Biot framework. They define the solid-solid contact as the boundary of two porous media at which they took the solid displacement field $(\mathrm{u}^{\mathrm{s}}_j)$, the total traction $(\tau_{jk}\hat{n}_k)$ and the normal component of the filtration velocity $(\dot{\mathrm{w}}_\perp)$ are continuous. The jump in fluid pressure $(\mathrm{p}^{\mathrm{f}})$ in their framework is dictated by the normal component of filtration velocity. The normal component of the filtration velocity is defined as porosity-weighted relative velocity of the fluid with respect to the solid. However, due to the redundancy of two degrees of freedom in the Biot framework, there is no description about what occurs with the filtration velocity in the tangential direction to the interface (Solorza and Sahay, 2009). The boundary conditions proposed by Deresiewicz and Skalak (1963) are

$$\left.\begin{array}{rcl} \left[\!\left[\mathrm{u}_j^{\mathrm{s}} \right]\!\right] & = & 0 \\ [\![\tau_{jk}\hat{n}_k]\!] & = & 0 \\ [\![\dot{\mathrm{w}}_\perp]\!] & = & 0 \\ \left[\!\left[\eta_0 \mathrm{p}^{\mathrm{f}} \right]\!\right] & = & \frac{1}{K_{DS}}\dot{\mathrm{w}}_\perp \end{array}\right\} \tag{52}$$

where $[\![\ ]\!]$ represent a jump in its argument. They include the parameter K_{DS}, called interface permeability, which describes the capability of fluid to move across the interface, and drives the jump in the fluid pressure over the interface.

For the case when a fluid is free to move, the open-pore case, they propose $K_{DS} = \infty$ such that there is no jump in fluid pressure. The counterpart impermeable condition, closed-pore case, is described by a zero interface permeability. That leads to vanishing normal component of the filtration velocity at the interface.

Gurevich and Schoenberg (1999) have shown that the open-pore boundary conditions proposed by Deresiewicz and Skalak (1963) are compatible with the Biot theory, but the impermeable case violates that framework and it is not possible to validate it from the differential operator. Also, Bourbie et al., (1987) argue that the Biot equation has to be modified such that the impermeability condition can be obtained from the differential operator. Solorza and Sahay (2009) pointed out that defining boundary conditions from the dCS framework avoids the mathematical inconsistency.

3.2 Adjoint boundary conditions of the dCS poroelastic wave equation

From (47), the dCS poroelastic wave operator $\hat{\mathbf{D}}$ is

$$\hat{\mathbf{D}} = \boldsymbol{\alpha}\nabla\left(\nabla\cdot\ \right) - \boldsymbol{\beta}\nabla\times(\nabla\times\ )\,, \tag{53}$$

which can be written as an eigenvalue problem,

$$\hat{\mathbf{D}}\,\mathbf{u} \;=\; -\,\omega^2\,\mathbf{u}. \tag{54}$$

It is apparent from equations (46) and (47) that the equivalent representation of the left hand side of equation (54) in terms of stresses is

$$\begin{aligned}
\hat{\mathbf{D}}\mathbf{u}_j &= \boldsymbol{\Omega}^{-1}\,\boldsymbol{\rho}^{-1}\boldsymbol{\tau}_{jk,k} \\
&= \begin{pmatrix} \frac{1}{\rho_{\mathrm{m}}} & 0 \\ 0 & \gamma_{_R}\frac{\mathrm{m_d^2}}{\rho_{\mathrm{i}}} \end{pmatrix} \begin{pmatrix} \tau^{\mathrm{m}}_{jk,k} \\ \tau^{\mathrm{i}}_{jk,k} \end{pmatrix} \text{ (using equations 29, 31, 50 and } \tfrac{1}{1+i\bar{\Omega}_{\mathrm{i}}/\omega} \equiv \gamma_{_R} \text{)} \\
&\equiv \begin{pmatrix} \Sigma^{\mathrm{m}}_{jk,k} \\ \Sigma^{\mathrm{i}}_{jk,k} \end{pmatrix} = \boldsymbol{\Sigma}_{jk,k}.
\end{aligned} \tag{55}$$

The above notation is introduced for the calculation of the adjoint operator.

Let $\mathbf{u}^{(1)}$ and $\mathbf{u}^{(2)}$ be arbitrary functions that are continuous and differentiable as required by the operator $\hat{\mathbf{D}}$. Both satisfy equation (54) in the domain V subjected to the same set of conditions on the bounding surface S of the domain V. Let the inner product of the two functions be defined by

$$<\,\mathbf{u}^{(1)}\,,\,\mathbf{u}^{(2)}\,> = \int_V \mathbf{u}^{(1)*}\,\cdot\,\mathbf{u}^{(2)} dV \tag{56}$$

where * stands for the complex conjugate. The adjoint of the differential operator $\mathbf{D}(\partial)$ is defined by the inner product of two functions as below (Friedman, 1962)

$$<\,\mathbf{u}^{(1)}\,,\,\hat{\mathbf{D}}\mathbf{u}^{(2)}\,> \;-\; <\,\hat{\mathbf{D}}\mathbf{u}^{(1)}\,,\,\mathbf{u}^{(2)}\,> = 0, \tag{57}$$

where $\hat{\mathbf{D}}^\dagger$ is the adjoint operator of $\hat{\mathbf{D}}$. In the following, the calculation for the adjoint operator $\hat{\mathbf{D}}^\dagger$ is carried out. The inner product of the first term of the left hand side of equation (57) is expressed as

$$
\begin{aligned}
< \mathbf{u}^{(1)}, \hat{\mathbf{D}}\mathbf{u}^{(2)} > &= \int_V \mathbf{u}^{(1)*} \cdot \left(\hat{\mathbf{D}}\mathbf{u}^{(2)}\right) dV, \\
&= \int_V \mathbf{u}_j^{(1)*} \cdot \left(\mathbf{\Sigma}_{jk,k}^{(2)}\right) dV, \text{ (using equation 55)} \\
&= \int_V \left\{ \Sigma_{jk,k}^{\mathrm{m}(2)} \ \mathrm{u}_j^{\mathrm{m}(1)^*} + \Sigma_{jk,k}^{\mathrm{i}(2)} \ \mathrm{u}_j^{\mathrm{i}(1)^*} \right\} dV. \qquad (58)
\end{aligned}
$$

By using the identity $\Sigma_{jk,k}^{\mathrm{m}} \, \mathrm{u}_j^{\mathrm{m}} = \left(\Sigma_{jk}^{\mathrm{m}} \, \mathrm{u}_j^{\mathrm{m}}\right)_{,k} - \Sigma_{kj}^{\mathrm{m}} \, \mathrm{u}_{j,k}^{\mathrm{m}}$, wherein on account of symmetry of stress tensor $\Sigma_{jk}^{\mathrm{m}} \, \mathrm{u}_{j,k}^{\mathrm{m}} = \Sigma_{jk}^{\mathrm{m}} \, \mathrm{u}_{jk}^{\mathrm{m}}$, and likewise the same identity for internal field term, the right hand of equation (58) becomes

$$
\begin{aligned}
\int_V \Big\{ \left(\Sigma_{jk}^{\mathrm{m}(2)} \ \mathrm{u}_j^{\mathrm{m}(1)^*}\right)_{,k} &+ \left(\Sigma_{jk}^{\mathrm{i}(2)} \ \mathrm{u}_j^{\mathrm{i}(1)^*}\right)_{,k} \\
&- \left(\Sigma_{jk}^{\mathrm{m}(2)} \ \mathrm{u}_{jk}^{\mathrm{m}(1)^*} + \Sigma_{jk}^{\mathrm{i}(2)} \ \mathrm{u}_{jk}^{\mathrm{i}(1)^*}\right) \Big\} \ dV, \qquad (59)
\end{aligned}
$$

in which the first two terms are converted, using Gauss's divergence theorem, into boundary terms

$$
\int_S \left(\Sigma_{jk}^{\mathrm{m}(2)} \ \mathrm{u}_j^{\mathrm{m}(1)^*} + \Sigma_{jk}^{\mathrm{i}(2)} \ \mathrm{u}_j^{\mathrm{i}(1)^*}\right) \hat{n}_k dS - \int_V \left(\Sigma_{jk}^{\mathrm{m}(2)} \ \mathrm{u}_{jk}^{\mathrm{m}(1)^*} + \Sigma_{jk}^{\mathrm{i}(2)} \ \mathrm{u}_{jk}^{\mathrm{i}(1)^*}\right) \ dV \qquad (60)
$$

where $\hat{n}_k$ is the unit normal to the surface S.

Using (51) and (55), the integrand of the volume integral in (60) is expressed as

$$
\begin{aligned}
\Sigma_{jk}^{\mathrm{m}(2)} \mathrm{u}_{jk}^{\mathrm{m}(1)^*} &= \left[(\alpha_{\mathrm{mm}} - 2\beta_{\mathrm{mm}}) \, \delta_{jk} \, \delta_{pq} \ + \ 2 \, \beta_{\mathrm{mm}} \, \delta_{jp} \, \delta_{kq}\right] \mathrm{u}_{pq}^{\mathrm{m}(2)} \, \mathrm{u}_{jk}^{\mathrm{m}(1)^*} + \\
&\quad \left[(\alpha_{\mathrm{mi}} - 2\beta_{\mathrm{mi}}) \, \delta_{jk} \, \delta_{pq} + 2\beta_{\mathrm{mi}} \, \delta_{jp} \, \delta_{kq}\right] \mathrm{u}_{pq}^{\mathrm{i}(2)} \, \mathrm{u}_{jk}^{\mathrm{m}(1)^*} \qquad (61)
\end{aligned}
$$

$$
\begin{aligned}
\Sigma_{jk}^{\mathrm{i}(2)} \mathrm{u}_{jk}^{\mathrm{i}(1)^*} &= \left[(\alpha_{\mathrm{im}} - 2\beta_{\mathrm{im}}) \, \delta_{jk} \, \delta_{pq} + 2 \, \beta_{\mathrm{im}} \, \delta_{jp} \, \delta_{kq}\right] \mathrm{u}_{pq}^{\mathrm{m}(2)} \, \mathrm{u}_{jk}^{\mathrm{m}(1)^*} + \\
&\quad \left[(\alpha_{\mathrm{ii}} - 2\beta_{\mathrm{ii}}) \, \delta_{jk} \, \delta_{pq} + 2\beta_{\mathrm{ii}} \, \delta_{jp} \, \delta_{kq}\right] \mathrm{u}_{pq}^{\mathrm{i}(2)} \, \mathrm{u}_{jk}^{\mathrm{m}(1)^*}. \qquad (62)
\end{aligned}
$$

Here, because of symmetric strain tensors and the symmetry of equations (61) and (62), it is

possible to interchange $\mathrm{u}_{jk}^{(1)^*}$ and $\mathrm{u}_{pq}^{(2)}$ without any effect.

The adjoint operator of $\hat{\mathbf{D}}$ is written as

$$\hat{\mathbf{D}}^{\dagger}\mathbf{u}_{j}^{(1)} \;=\; \begin{pmatrix} \Sigma_{jk,k}^{\dagger \mathrm{m}^{(1)}} \\ \Sigma_{jk,k}^{\dagger \mathrm{i}^{(1)}} \end{pmatrix} = \;\; \mathbf{\Sigma}_{jk,k}^{\dagger(1)}. \tag{63}$$

Using the above structure, the inner product of the second term of the left hand of equation (57) is now expressed as

$$\int_S \left\{ \Sigma_{jk}^{\dagger \mathrm{m}(1)^*} \mathrm{u}_j^{\mathrm{m}(2)} + \Sigma_{jk}^{\dagger \mathrm{i}(1)^*} \mathrm{u}_j^{\mathrm{i}(2)} \right\} \hat{n}_k dS - \int_V \left\{ \Sigma_{jk}^{\dagger \mathrm{m}(1)^*} \mathrm{u}_{jk}^{m(2)} + \Sigma_{jk}^{\dagger \mathrm{i}(1)^*} \mathrm{u}_{jk}^{\mathrm{i}(2)} \right\} dV \tag{64}$$

From (60) and (64), the left hand side of (57) becomes

$$\int_S \left\{ \Sigma_{jk}^{\mathrm{m}(2)} \; \mathrm{u}_j^{\mathrm{m}(1)^*} + \Sigma_{jk}^{\mathrm{i}(2)} \; \mathrm{u}_j^{\mathrm{i}(1)^*} - \Sigma_{jk}^{\dagger \mathrm{m}(1)^*} \mathrm{u}_j^{\mathrm{m}(2)} - \Sigma_{jk}^{\dagger \mathrm{i}(1)^*} \mathrm{u}_j^{\mathrm{i}(2)} \right\} n_k dS -$$

$$\int_V \left\{ \Sigma_{jk}^{\mathrm{m}(2)} \; \mathrm{u}_{jk}^{\mathrm{m}(1)^*} + \Sigma_{jk}^{\mathrm{i}(2)} \; \mathrm{u}_{jk}^{\mathrm{i}(1)^*} - \Sigma_{jk}^{\dagger \mathrm{m}(1)^*} \mathrm{u}_{jk}^{\mathrm{m}(2)} - \Sigma_{jk}^{\dagger \mathrm{i}(1)^*} \mathrm{u}_{jk}^{\mathrm{i}(2)} \right\} dV \,. \tag{65}$$

In order to validate the identity (57), the above sum must vanish.

In expressions (61) and (62), upon interchanging $\mathrm{u}_{jk}^{(1)^*}$ and $\mathrm{u}_{pq}^{(2)}$, and further algebraic manipulation leads to

$$\begin{aligned} \Sigma_{jk}^{\dagger \mathrm{m}(1)^*} \;\; = \;\; & \left[(\alpha_{\mathrm{mm}} - 2\beta_{\mathrm{mm}}) \, \delta_{jk} \, \delta_{pq} + 2 \, \beta_{\mathrm{mm}} \, \delta_{jp} \, \delta_{kq} \right] \mathrm{u}_{pq}^{\mathrm{m}(1)^*} + \\ & \left[(\alpha_{\mathrm{im}} - 2\beta_{\mathrm{im}}) \, \delta_{jk} \, \delta_{lm} + 2 \, \beta_{\mathrm{im}} \, \delta_{jl} \, \delta_{km} \right] \mathrm{u}_{lm}^{\mathrm{i}(1)^*}, \end{aligned} \tag{66}$$

$$\begin{aligned} \Sigma_{jk}^{\dagger \mathrm{i}(1)^*} \;\; = \;\; & \left[(\alpha_{\mathrm{mi}} - 2\beta_{\mathrm{mi}}) \, \delta_{jk} \, \delta_{pq} + 2 \, \beta_{\mathrm{mi}} \, \delta_{jp} \, \delta_{kq} \right] \mathrm{u}_{pq}^{\mathrm{m}(1)^*} + \\ & \left[(\alpha_{\mathrm{ii}} - 2\beta_{\mathrm{ii}}) \, \delta_{jk} \, \delta_{pq} + 2 \, \beta_{\mathrm{ii}} \, \delta_{jp} \, \delta_{kq} \right] \mathrm{u}_{pq}^{\mathrm{i}(1)^*}. \end{aligned} \tag{67}$$

The expressions (61), (62), (66) and (67) indeed allow the volume integral term in (65) to vanish. Thus, for the dCS wave operator to be adjoint, the boundary conditions must be such that the surface integral in (65) also vanishes.

Using the fact that both the dCS operator $\hat{\mathbf{D}}$ and its adjoint $\hat{\mathbf{D}}^{\dagger}$ are subjected to the same set of conditions on the bounding surface S of the domain V, changing the notation (from $\boldsymbol{\Sigma}$ to $\boldsymbol{\tau}$) and specializing for the case cylindrical coordinate system with the unit normal to the surface taken in radial direction, the following choice of boundary conditions must hold true

$$\left.\begin{aligned} \tau^{\mathrm{m}}_{rr}\mathrm{u}^{m}_{r} &= 0 \\ \tau^{\mathrm{m}}_{rz}\mathrm{u}^{m}_{z} &= 0 \\ \tau^{\mathrm{i}}_{rr}\mathrm{u}^{i}_{r} &= 0 \\ \tau^{\mathrm{i}}_{rz}\mathrm{u}^{i}_{z} &= 0 \end{aligned}\right\} \tag{68}$$

so that the surface integral in (65) vanishes and allows the dCS wave operator to have an adjoint.

Equations (68) describes sixteen sets of the homogeneous boundary conditions that allow to have the adjoint operator for the dCS wave operator.

3.3 Stress-free impermeable boundary conditions

The stress-free condition at the boundary describes the state wherein there are no forces acting on the totality of the poro-continuum. That requires the tractions corresponding to the sum total of phasic stresses vanishing at the boundary, i.e., mean or total stress in the normal and tangential directions to the surface must be set to zero. For the case of cylindrical coordinate system, with the unit normal to the surface S taken in radial direction, the stress-free boundary condition must read as

$$\tau^{\mathrm{m}}_{rr_{|S}} = 0, \tag{69}$$

$$\tau^{\mathrm{m}}_{rz_{|S}} = 0. \tag{70}$$

The impermeability of a surface means that no fluid is allowed to move across it. This requires

that in direction normal to surface both phases must move in unison, i.e., there can not be relative motion of phases in the direction perpendicular to the interface. Thus, the normal component of the internal field must vanish at the interface since it is precisely the difference in motion of phases, that is,

$$\mathrm{u}^{\mathrm{i}}_{r_{|S}} \quad = \quad 0. \tag{71}$$

The conditions (69) through (71) automatically satisfy the first three conditions of (68). The last condition of (68) can be satisfied by either $\mathrm{u}^{\mathrm{i}}_{z_{|S}} = 0$ or $\tau^{\mathrm{i}}_{rz_{|S}} = 0$ to ensure that this set is an adjoint boundary condition for the dCS wave operator.

$\mathrm{u}^{\mathrm{i}}_{z_{|S}} = 0$ describes the state where, at the surface, the fluid is forced to move in unison with the solid in the tangential direction. However, this condition does not have a physical meaning because keeping the fluid welded to the solid at the interface in the tangential direction is physically impossible.

Conversely, the choice of

$$\tau^{\mathrm{i}}_{rz_{|S}} = 0 \tag{72}$$

means that the tangential components of phasic stresses are balanced at the interface in the tangential direction, which amounts to no restrictions on the relative motion in that direction. This condition has a physical meaning. It is because together with the condition (70), it amounts to maintaining the tangential components of stress of both phases vanished at the surface, which is realistic.

Thus, the set of conditions (69) through (72) are the proper boundary condition for a stress-free impermeable surface.

Chapter 4 Longitudinal motion with stress-free impermeable radial surface

Longitudinal motion has displacements only in axial $(\mathbf{u}_z)$ and radial $(\mathbf{u}_r)$ directions and they are independent of azimuth. As there is no azimuthal component of displacement, it is a 2D motion.

The governing equations of longitudinal motion of a poroelastic cylinder are presented in §4.1. Thereafter, the associated set of boundary conditions on the radial surface of cylinder, which hold it stress-free and impermeable, are stated in §4.2. In §4.3 the equations of motion are decoupled using a generalization of Hansen vectors[1]. That leads to a set of fours scalar potentials, each governed by a Helmholtz equation. Solutions for these potentials are constructed in terms of a complete set of orthogonal cylindrical and trigonometric functions. Following that expressions of displacements and stresses are developed in terms of these decoupled potentials in §4.4. After that in §4.5 the system of equations satisfying boundary conditions at the radial surface are setup and the resulting dispersion polynomial is developed in §4.6.

The methodology and notations adopted here are common to Solorza and Sahay (2009) who have carried out the dispersion analysis of longitudinal motion of poroelastic circular cylinder with stress-free and permeable radial surface.

4.1 Governing equations

The longitudinal waves have a cylindrical symmetry independent of the azimuth, so the poroelastic equations of motion in frequency domain (46) become

$$\boldsymbol{\Omega}^{-1}\boldsymbol{\rho}^{-1}\left(\boldsymbol{\tau}_{rz,z}+\boldsymbol{\tau}_{rr,r}+\frac{1}{r}\left(\boldsymbol{\tau}_{rr}-\tau_{\theta\theta}\right)\right)+\omega^2\mathbf{u}_r \;=\; 0, \tag{73}$$

$$\boldsymbol{\Omega}^{-1}\boldsymbol{\rho}^{-1}\left(\boldsymbol{\tau}_{zz,z}+\boldsymbol{\tau}_{rz,r}+\frac{1}{r}\boldsymbol{\tau}_{rz}\right)+\omega^2\mathbf{u}_z \;=\; 0\,, \tag{74}$$

[1] Hansen's vector wave functions have origin in electro-magnetism and later adopted to linear elasticity. Its historical account is in Senior (1960).

where $\boldsymbol{\rho}$ and $\boldsymbol{\Omega}$ are the density and the Rayleigh damping matrices defined in (31) and (50), respectively. From (51) the corresponding stresses are

$$\boldsymbol{\tau}_{rr} = \boldsymbol{\Omega\rho}\left((\boldsymbol{\alpha}-2\boldsymbol{\beta})\left[\left(\partial_r+\frac{1}{r}\right)\mathbf{u}_r+\partial_z\mathbf{u}_z\right]+2\boldsymbol{\beta}\partial_r\mathbf{u}_r\right) \quad , \tag{75}$$

$$\boldsymbol{\tau}_{zz} = \boldsymbol{\Omega\rho}\left((\boldsymbol{\alpha}-2\boldsymbol{\beta})\left[\left(\partial_r+\frac{1}{r}\right)\mathbf{u}_r+\partial_z\mathbf{u}_z\right]+2\boldsymbol{\beta}\partial_z\mathbf{u}_z\right) \quad , \tag{76}$$

$$\boldsymbol{\tau}_{\theta\theta} = \boldsymbol{\Omega\rho}\left((\boldsymbol{\alpha}-2\boldsymbol{\beta})\left[\left(\partial_r+\frac{1}{r}\right)\mathbf{u}_r+\partial_z\mathbf{u}_z\right]+2\boldsymbol{\beta}\frac{\mathbf{u}_r}{r}\right) \quad , \tag{77}$$

$$\boldsymbol{\tau}_{rz} = \boldsymbol{\Omega\rho\beta}\left(\partial_z\mathbf{u}_r+\partial_r\mathbf{u}_z\right). \tag{78}$$

$\boldsymbol{\alpha}$ and $\boldsymbol{\beta}$ are the 2×2 matrices associated with the P and S wave motion defined in equations (48) and (49), respectively.

Substituting in (75) through (78) in (73) and (74), the equations of motion, in terms of displacement fields only, are written as

$$\boldsymbol{\alpha}\nabla(\nabla\cdot\mathbf{u})-\boldsymbol{\beta}\nabla\times\nabla\times\mathbf{u}+\omega^2\mathbf{u} = 0 \tag{79}$$

where $\mathbf{u}=(\mathbf{u}_r\ \mathbf{u}_z)^T$.

4.2 Boundary conditions

The case of a stress-free impermeable radial surface means that the tractions corresponding to total stress vanish and the fluid is not capable of moving in and out of the radial surface. These conditions are described by the set of conditions (69) through (72) developed in §3.3

$$\left.\begin{array}{rcl} \tau^{\mathrm{m}}_{rr_{|r=a}} & = & 0 \\ \tau^{\mathrm{m}}_{rz_{|r=a}} & = & 0 \\ \tau^{\mathrm{i}}_{rz_{|r=a}} & = & 0 \\ \mathrm{u}^{\mathrm{i}}_{r_{|r=a}} & = & 0, \end{array}\right\} \tag{80}$$

which are re-expressed in terms the extended variables notation as

$$\left.\begin{array}{rcl} \hat{\mathbf{P}}_1\,\boldsymbol{\tau}_{rz_{|r=a}} & = & 0 \\ \hat{\mathbf{P}}_1\,\boldsymbol{\tau}_{rr_{|r=a}} & = & 0 \\ \hat{\mathbf{P}}_2\,\boldsymbol{\tau}_{rz_{|r=a}} & = & 0 \\ \hat{\mathbf{P}}_2\,\mathbf{u}_{r_{|r=a}} & = & 0 \end{array}\right\}. \tag{81}$$

Here $\hat{\mathbf{P}}_1 = (1 \;\; 0)$ and $\hat{\mathbf{P}}_2 = (0 \;\; 1)$ are the projection operators which allow the extraction of the 1st row (the centre-of-mass field terms) and the 2nd row (the internal field terms), respectively.

4.3 Decoupling of equations of motion by potentials

For the longitudinal case the displacement field $\mathbf{u}$ is independent of azimuth and there is no azimuthal component of displacement, the equations of longitudinal motion (79) are decoupled using generalized Hansen vectors as below

$$\mathbf{u} \;\; = \;\; \mathbf{L} + \mathbf{N}, \quad \text{and } \mathbf{L} = \nabla\boldsymbol{\Phi}, \quad \mathbf{N} = \nabla \times \nabla \times (\hat{z}\boldsymbol{\Xi}) \tag{82}$$

where potentials are column vectors composed by two elements. They are

$$\boldsymbol{\Phi} \;\; = \;\; \left(\Phi^{\mathrm{m}} \;\; \Phi^{\mathrm{i}}\right)^{\mathrm{T}}, \tag{83}$$

$$\boldsymbol{\Xi} \;\; = \;\; \left(\chi^{\mathrm{m}} \;\; \chi^{\mathrm{i}}\right)^{\mathrm{T}}. \tag{84}$$

Applying the Hansen vector decomposition (82) in equation (79) and using the identity $\nabla^2 = \nabla\left(\nabla\cdot\right) - \nabla\times\left(\nabla\times\right)$, the curl-free (compressional) and divergence-free (shear) parts are separated.

Each is governed by a 2×2 matrix Helmholtz equation as

$$\boldsymbol{\alpha}\nabla^2\boldsymbol{\Phi}+\omega^2\boldsymbol{\Phi} \;=\; 0 \tag{85}$$

$$\boldsymbol{\beta}\nabla^2\boldsymbol{\Xi}+\omega^2\boldsymbol{\Xi} \;=\; 0 \tag{86}$$

Equations (85) and (86) are 2×2 coupled system of equations. The coupling is because of the non-symmetric $\boldsymbol{\alpha}$ and $\boldsymbol{\beta}$ matrices. In order to decouple, their right- and left- eigenvector matrices are constructed, which are developed in the sections below. Although, the eigenvalues of a nonsymetric matrix $\mathbf{A}$ and its transpose $\mathbf{A}^{\mathrm{T}}$ are the same, but their eigenvectors are different. They are called the right- and left- eigenvectors of matrix $\mathbf{A}$.

4.3.1 Solution of the matrix Helmholtz equations for compressional waves

The matrix Helmholtz equation for compressional waves (85) is diagonalized by introducing the transformation

$$\boldsymbol{\Phi}=\mathbf{R}_\alpha\boldsymbol{\phi} \tag{87}$$

where

$$\boldsymbol{\phi}=(\phi^{\mathrm{I}}\quad\phi^{\mathrm{II}})^{\mathrm{T}}, \tag{88}$$

$$\mathbf{R}_\alpha \;=\; \begin{pmatrix}\mathbf{r}_{\alpha_{\mathrm{I}}} & \mathbf{r}_{\alpha_{\mathrm{II}}}\end{pmatrix} \tag{89}$$

and

$$\mathbf{L}_\alpha \;=\; \begin{pmatrix}\mathbf{l}_{\alpha_{\mathrm{I}}} & \mathbf{l}_{\alpha_{\mathrm{II}}}\end{pmatrix}. \tag{90}$$

$\mathbf{R}_\alpha$ and $\mathbf{L}_\alpha$ are, respectively, right- and left- eigenvector matrices of the non-symmetric second order $\boldsymbol{\alpha}$ matrix such that they are orthonormal to each other,

$$\mathbf{L}_\alpha^{\mathrm{T}}\,\mathbf{R}_\alpha=\mathbf{I}, \tag{91}$$

where their components are defined as

$$\mathbf{r}_{\alpha_{\mathrm{I}}} = \frac{1}{\mathrm{N}_{\alpha_{\mathrm{I}}}} \begin{pmatrix} 1 \\ \gamma_{\alpha_{\mathrm{I}}} \end{pmatrix} \text{ and } \mathbf{r}_{\alpha_{\mathrm{II}}} = \frac{1}{\mathrm{N}_{\alpha_{\mathrm{II}}}} \begin{pmatrix} \gamma_{\alpha_{\mathrm{II}}} \\ 1 \end{pmatrix} \tag{92}$$

and

$$\mathbf{l}_{\alpha_{\mathrm{I}}} = \frac{1}{\mathrm{N}_{\alpha_{\mathrm{I}}}} \begin{pmatrix} 1 \\ \gamma_{\alpha_{\mathrm{I}}} \frac{\alpha_{\mathrm{mi}}}{\alpha_{\mathrm{im}}} \end{pmatrix} \text{ and } \mathbf{l}_{\alpha_{\mathrm{II}}} = \frac{1}{\mathrm{N}_{\alpha_{\mathrm{II}}}} \begin{pmatrix} \gamma_{\alpha_{\mathrm{II}}} \frac{\alpha_{\mathrm{im}}}{\alpha_{\mathrm{mi}}} \\ 1 \end{pmatrix}, \tag{93}$$

with $\gamma_{\alpha_{\mathrm{I}}} = (\alpha_{\mathrm{I}}^2 - \alpha_{\mathrm{mm}})/\alpha_{\mathrm{mi}}$ and $\gamma_{\alpha_{\mathrm{II}}} = \alpha_{\mathrm{mi}}/(\alpha_{\mathrm{II}}^2 - \alpha_{\mathrm{mm}})$. $\mathrm{N}_{\alpha_{\mathrm{I}}} = \left(1 + \gamma_{\alpha_{\mathrm{I}}}^2 \alpha_{\mathrm{mi}}/\alpha_{\mathrm{im}}\right)^{1/2}$ and $\mathrm{N}_{\alpha_{\mathrm{II}}} = \left(1 + \gamma_{\alpha_{\mathrm{II}}}^2 \alpha_{\mathrm{im}}/\alpha_{\mathrm{mi}}\right)^{1/2}$ are normalizations constants.

$\mathbf{R}_\alpha$ and $\mathbf{L}_\alpha$ diagonalize the $\boldsymbol{\alpha}$ matrix,

$$\mathbf{L}_\alpha^{\mathrm{T}}\, \boldsymbol{\alpha}\, \mathbf{R}_\alpha = \boldsymbol{\Lambda}_\alpha \equiv \begin{pmatrix} \alpha_{\mathrm{I}}^2 & 0 \\ 0 & \alpha_{\mathrm{II}}^2 \end{pmatrix}, \tag{94}$$

where $(\alpha_{\mathrm{I}}^2 \text{ and } \alpha_{\mathrm{II}}^2)$ are the eigenvalues of the $\boldsymbol{\alpha}$ matrix.

Applying the transformation (87) into equation (85), followed by the application of $\mathbf{L}_\alpha^{\mathrm{T}}$ from the left and using the identities (91) and (94), the set of two decoupled scalar Helmholtz equations for $\boldsymbol{\phi}$ are

$$\boldsymbol{\Lambda}_{\boldsymbol{\alpha}} \nabla^2 \boldsymbol{\phi} + \omega^2 \boldsymbol{\phi} = \mathbf{0}. \tag{95}$$

The elementary solutions of these Helmholtz equations, in cylindrical coordinates, are taken in terms trigonometric and Bessel functions in axial and radial directions, respectively. Due to the angular independence of the motion in longitudinal problems, for the radial component only a Bessel function of order zero is allowed. Furthermore, the Bessel function of second kind must be dropped because of its singularity at the origin.

The elementary solution of (95) is

$$\boldsymbol{\phi} = \begin{pmatrix} \phi^{\mathrm{I}} \\ \phi^{\mathrm{II}} \end{pmatrix} = \begin{pmatrix} J_0\left(q_{\alpha_{\mathrm{I}}} r\right) & 0 \\ 0 & J_0\left(q_{\alpha_{\mathrm{II}}} r\right) \end{pmatrix} e^{ikz} \begin{pmatrix} a_{\mathrm{I}} \\ a_{\mathrm{II}} \end{pmatrix}, \tag{96}$$

where $q_{\alpha_{\mathrm{I}}}, q_{\alpha_{\mathrm{II}}}$ are the radial wave numbers P-waves. They are

$$q_{\alpha_{\mathrm{I}}} = \sqrt{\frac{\omega^2}{\alpha_{\mathrm{I}}^2} - k^2}, \qquad q_{\alpha_{\mathrm{II}}} = \sqrt{\frac{\omega^2}{\alpha_{\mathrm{II}}^2} - k^2}, \tag{97}$$

and the imaginary part of the radial wave numbers must be taken such that the Sommerfeld radiation condition is satisfied in the manner suggested by Krebes and Daley (2007).

The solutions of two decoupled potentials are written jointly in a matrix form for algebraic convenience. The axial wave number k is the free parameter. The elementary solutions are labeled by the pair (k, ω). They are to be viewed as the Fourier spatial and temporal wave-numbers. By imposing the boundary conditions (81) the interrelation between these wave-numbers is yet to determined by the dispersion analysis.

4.3.2 Solution of the matrix Helmholtz equations for shear waves

Likewise the precceding §4.3.1, the matrix Helmholtz equation for shear waves (86) is diagonalized by introducing the transformation

$$\boldsymbol{\Xi} = \mathbf{R}_\beta \boldsymbol{\chi} \tag{98}$$

with

$$\boldsymbol{\chi} = (\chi^{\mathrm{I}} \;\; \chi^{\mathrm{II}})^{\mathrm{T}} \tag{99}$$

$$\mathbf{R}_\beta = \begin{pmatrix} \mathbf{r}_{\beta_{\mathrm{I}}} & \mathbf{r}_{\beta_{\mathrm{II}}} \end{pmatrix} \tag{100}$$

and

$$\mathbf{L}_\beta = \begin{pmatrix} \mathbf{l}_{\beta_{\mathrm{I}}} & \mathbf{l}_{\beta_{\mathrm{II}}} \end{pmatrix} \tag{101}$$

where $\mathbf{R}_\beta$ and $\mathbf{L}_\beta$ are, respectively, right- and left- eigenvector matrices of the non-symmetric second order $\boldsymbol{\beta}$ matrix and they are orthonormal to each other,

$$\mathbf{L}_\beta^{\mathrm{T}}\,\mathbf{R}_\beta = \mathbf{I}, \tag{102}$$

where their components are

$$\mathbf{r}_{\beta_{\mathrm{I}}} = \frac{1}{\mathrm{N}_{\beta_{\mathrm{I}}}}\begin{pmatrix} 1 \\ \gamma_{\beta_{\mathrm{I}}} \end{pmatrix} \text{ and } \mathbf{r}_{\beta_{\mathrm{II}}} = \frac{1}{\mathrm{N}_{\beta_{\mathrm{II}}}}\begin{pmatrix} \gamma_{\beta_{\mathrm{II}}} \\ 1 \end{pmatrix} \tag{103}$$

and

$$\mathbf{l}_{\beta_{\mathrm{I}}} = \frac{1}{\mathrm{N}_{\beta_{\mathrm{I}}}}\begin{pmatrix} 1 \\ \gamma_{\beta_{\mathrm{I}}}\frac{\beta_{\mathrm{mi}}}{\beta_{\mathrm{im}}} \end{pmatrix} \text{ and } \mathbf{l}_{\beta_{\mathrm{II}}} = \frac{1}{\mathrm{N}_{\beta_{\mathrm{II}}}}\begin{pmatrix} \gamma_{\beta_{\mathrm{II}}}\frac{\beta_{\mathrm{im}}}{\beta_{\mathrm{mi}}} \\ 1 \end{pmatrix}, \tag{104}$$

with $\gamma_{\beta_{\mathrm{I}}} = (\beta_{\mathrm{I}}^2 - \beta_{\mathrm{mm}})/\beta_{\mathrm{mi}}$ and $\gamma_{\beta_{\mathrm{II}}} = \beta_{\mathrm{mi}}/(\beta_{\mathrm{II}}^2 - \beta_{\mathrm{mm}})$. $\mathrm{N}_{\beta_{\mathrm{I}}} = \left(1+\gamma_{\beta_{\mathrm{I}}}^2\beta_{\mathrm{mi}}/\beta_{\mathrm{im}}\right)^{1/2}$ and $\mathrm{N}_{\beta_{\mathrm{II}}} = \left(1+\gamma_{\beta_{\mathrm{II}}}^2\beta_{\mathrm{im}}/\beta_{\mathrm{mi}}\right)^{1/2}$ are normalizations constants.

$\mathbf{R}_\beta$ and $\mathbf{L}_\beta$ diagonalize the $\boldsymbol{\beta}$ matrix,

$$\mathbf{L}_\beta^{\mathrm{T}}\,\boldsymbol{\beta}\,\mathbf{R}_\beta = \boldsymbol{\Lambda}_\beta \equiv \begin{pmatrix} \beta_{\mathrm{I}}^2 & 0 \\ 0 & \beta_{\mathrm{II}}^2 \end{pmatrix}. \tag{105}$$

where $\beta_{\mathrm{I}}^2 \text{ and } \beta_{\mathrm{II}}^2$ are the eigenvalues of the $\boldsymbol{\beta}$ matrix.

Applying the transformation (98) into equation (86) followed by the application of $\mathbf{L}_\beta^{\mathrm{T}}$ from the left side, as in the compressional case, this becomes a set of two decoupled scalar Helmholtz equations for $\boldsymbol{\chi}$

$$\boldsymbol{\Lambda}_{\boldsymbol{\alpha}}\nabla^2\boldsymbol{\chi} + \omega^2\boldsymbol{\chi} = \mathbf{0}. \tag{106}$$

The elementary solutions of (106) are given, akin to equation (95), in terms of trigonometric and zeroth-order Bessel functions as

$$\boldsymbol{\chi} = \begin{pmatrix} \chi^{\mathrm{I}} \\ \chi^{\mathrm{II}} \end{pmatrix} = \begin{pmatrix} J_0\left(q_{\beta_{\mathrm{I}}} r\right) & 0 \\ 0 & J_0\left(q_{\beta_{\mathrm{II}}} r\right) \end{pmatrix} e^{ikz} \begin{pmatrix} b_{\mathrm{I}} \\ b_{\mathrm{II}} \end{pmatrix}, \tag{107}$$

where $q_{\beta_{\mathrm{I}}}$, $q_{\beta_{\mathrm{II}}}$ are the radial wave numbers for shear waves given by

$$q_{\beta_{\mathrm{I}}} = \sqrt{\frac{\omega^2}{\beta_{\mathrm{I}}^2} - k^2}, \qquad q_{\beta_{\mathrm{II}}} = \sqrt{\frac{\omega^2}{\beta_{\mathrm{II}}^2} - k^2}. \tag{108}$$

4.4 Expressions of displacements and stresses in terms of potentials

From equations (87) and (98) substituting in equation (82) and followed by some algebraic manipulations, the expressions for radial and axial deformations in terms of the decoupling potentials ϕ and $\boldsymbol{\chi}$ are given by

$$\mathbf{u}_r = \mathbf{R}_\alpha \partial_r \boldsymbol{\phi} + \mathbf{R}_\beta \partial_{rz}^2 \boldsymbol{\chi}, \tag{109}$$

$$\mathbf{u}_z = \mathbf{R}_\alpha \partial_z \boldsymbol{\phi} - \mathbf{R}_\beta \left(\partial_r^2 + \frac{1}{r}\partial_r\right) \boldsymbol{\chi}, \tag{110}$$

and, likewise, from equations (75) and (78) stresses are

$$\boldsymbol{\tau}_{rr} = \boldsymbol{\Omega\rho\beta} \left\{ \left[\left(\boldsymbol{\beta}^{-1}\boldsymbol{\alpha} - 2\right) \mathbf{R}_\alpha \nabla^2 + 2\mathbf{R}_\alpha \partial_r^2 \right] \boldsymbol{\phi} + 2\mathbf{R}_\beta \partial_r^2 \partial_z \boldsymbol{\chi} \right\}, \tag{111}$$

$$\boldsymbol{\tau}_{rz} = \boldsymbol{\Omega\rho\beta} \left\{ 2\mathbf{R}_\alpha \partial_{rz}^2 \boldsymbol{\phi} + \mathbf{R}_\beta \partial_r \left[\partial_z^2 - \left(\partial_r^2 + \frac{1}{r}\partial_r\right) \right] \boldsymbol{\chi} \right\}. \tag{112}$$

Substituting (96) and (107) into the above equations, the displacements and stresses become

$$\mathbf{u}_r = -\frac{r}{2ik}\left[\frac{1}{k^2}\mathbf{R}_\alpha\mathbf{Q}_\alpha\mathbf{\Theta}_\alpha\mathbf{\Lambda}_\alpha\mathbf{A}-2\mathbf{R}_{_\beta}\mathbf{\Theta}_{_\beta}\mathbf{\Lambda}_{_\beta}\mathbf{B}\right]e^{ikz}, \tag{113}$$

$$\mathbf{u}_z = \frac{1}{k^2}\left[\mathbf{R}_\alpha\mathbf{\Lambda}_\alpha\mathbf{A}+2\mathbf{R}_{_\beta}\mathbf{\Lambda}_{_\beta}\mathbf{B}\right]e^{ikz}, \tag{114}$$

$$\begin{aligned}\boldsymbol{\tau}_{rr} = &-\frac{\mathbf{\Omega}\boldsymbol{\rho}\boldsymbol{\beta}}{ik}\left[\left\{\left(\boldsymbol{\beta}^{-1}\boldsymbol{\alpha}-2\right)\mathbf{R}_\alpha\frac{\omega^2}{k^2}+2\mathbf{R}_\alpha\left(\frac{\omega^2}{k^2}\mathbf{I}-\mathbf{\Lambda}_\alpha\right)\left(\mathbf{I}-\frac{1}{2}\mathbf{\Theta}_\alpha\right)\right\}\mathbf{A}\right.\\ &\left.-2\mathbf{R}_{_\beta}\mathbf{\Lambda}_{_\beta}\left(2\mathbf{I}-\mathbf{\Theta}_{_\beta}\right)\mathbf{B}\right]e^{ikz},\end{aligned} \tag{115}$$

$$\boldsymbol{\tau}_{rz} = -r\mathbf{\Omega}\boldsymbol{\rho}\boldsymbol{\beta}\left[\mathbf{R}_\alpha\left(\frac{\omega^2}{k^2}\mathbf{I}-\mathbf{\Lambda}_\alpha\right)\mathbf{\Theta}_\alpha\mathbf{A}+\mathbf{R}_{_\beta}\left(\frac{\omega^2}{k^2}-2\mathbf{\Lambda}_{_\beta}\right)\mathbf{\Theta}_{_\beta}\mathbf{B}\right]e^{ikz}, \tag{116}$$

where $\mathbf{Q}_\alpha$, $\mathbf{Q}_{_\beta}$, $\mathbf{\Theta}_\alpha$, $\mathbf{\Theta}_{_\beta}$ are diagonal 2×2 matrices and $\mathbf{A}$, $\mathbf{B}$ are two-component vectors. These are defined in terms of their components as

$$\begin{pmatrix} q_{\alpha_I}^2 & 0 \\ 0 & q_{\alpha_{II}}^2 \end{pmatrix} \equiv \boldsymbol{Q}_\alpha \tag{117}$$

$$\begin{pmatrix} q_{\beta_I}^2 & 0 \\ 0 & q_{\beta_{II}}^2 \end{pmatrix} \equiv \boldsymbol{Q}_\beta \tag{118}$$

$$\begin{pmatrix} \frac{2J_1(q_{\alpha_I}r)}{rq_{\alpha_I}J_0(q_{\alpha_I}r)} & 0 \\ 0 & \frac{2J_1(q_{\alpha_{II}}r)}{rq_{\alpha_{II}}J_0(q_{\alpha_{II}}r)} \end{pmatrix} \equiv \begin{pmatrix} \Theta(q_{\alpha_I}r) & 0 \\ 0 & \Theta(q_{\alpha_{II}}r) \end{pmatrix} \equiv \mathbf{\Theta}_\alpha \tag{119}$$

$$\begin{pmatrix} \frac{2J_1(q_{\beta_I}r)}{rq_{\beta_I}J_0(q_{\beta_I}r)} & 0 \\ 0 & \frac{2J_1(q_{\beta_{II}}r)}{rq_{\beta_{II}}J_0(q_{\beta_{II}}r)} \end{pmatrix} \equiv \begin{pmatrix} \Theta(q_{\beta_I}r) & 0 \\ 0 & \Theta(q_{\beta_{II}}r) \end{pmatrix} \equiv \mathbf{\Theta}_\beta \tag{120}$$

$$ik^3\left(\mathbf{\Lambda}_\alpha\right)^{-1}\begin{pmatrix} J_0(q_{\alpha_I}r) & 0 \\ 0 & J_0(q_{\alpha_{II}}r) \end{pmatrix}\begin{pmatrix} a_I \\ a_{II} \end{pmatrix} \equiv \begin{pmatrix} A_I \\ A_{II} \end{pmatrix} \equiv \boldsymbol{A} \tag{121}$$

$$\frac{1}{2}k^2\left(\mathbf{\Lambda}_\beta\right)^{-1}\boldsymbol{Q}_\beta\begin{pmatrix} J_0(q_{\beta_I}r) & 0 \\ 0 & J_0(q_{\beta_{II}}r)\end{pmatrix}\begin{pmatrix} b_I \\ b_{II}\end{pmatrix}\equiv\begin{pmatrix} B_I \\ B_{II}\end{pmatrix}\equiv\boldsymbol{B} \tag{122}$$

It is to be noted that cylindrical function $\mathbf{\Theta}_\alpha$ ($\mathbf{\Theta}_\beta$) and coefficient $\mathbf{A}$ ($\mathbf{B}$) are divided and multiplied by zeroth-order Bessel function, respectively. The scaling of the cylindrical functions are for algebraic convenience in dispersion analysis. This analytic manipulation traces back to the works of *Pochhammer* and *Chere* in the late eighteenth century on vibration of elastic cylinders.

4.5 Setting up the boundary conditions

The boundary conditions for a stress-free impermeable surface are defined in (81). They are explicitly stated in terms of extended variables notations for displacement fields and stresses in equations (113), (115) and (116). From them the centre-mass- and internal- field components are extracted by apply the projection vectors from the left side to the desired expression. The projection operators are the row matrices as below

$$\hat{\mathbf{P}}_1 = (1\ \ 0)\,, \tag{123}$$

$$\hat{\mathbf{P}}_2 = (0\ \ 1)\,, \tag{124}$$

where $\hat{\mathbf{P}}_1$ extracts the 1st row which corresponds to the centre-mass field terms and $\hat{\mathbf{P}}_2$ extracts the 2nd row corresponding to the internal field terms. These are the same operators defined earlier in equation (81).

The boundary conditions on the radial surface $r = a$ are satisfied by applying the operator $\hat{\mathbf{P}}_1$ on equation (115), (116) and operator $\hat{\mathbf{P}}_2$ on equation (113) and (116) and setting $r = a$ in the resulting expressions. Here onwards, the notations $\frac{\omega^2}{k^2} \equiv V^2$, $\mathbf{\Theta}_\alpha|_{r=a} \equiv \mathbf{\Theta}^a_\alpha$ and $\mathbf{\Theta}_\beta|_{r=a} \equiv \mathbf{\Theta}^a_\beta$ are used.

Applying operator $\hat{\mathbf{P}}_1$ on equation (116) and setting $r = a$ yields

$$\tau^m_{rz|_{r=a}} \;=\; \hat{\mathbf{P}}_1\,\mathbf{R}_\beta\,\Big(\mathbf{\Lambda}_\beta\,\mathbf{L}^T_\beta\,\mathbf{R}_\alpha\,\left(V^2\mathbf{I}-\mathbf{\Lambda}_\alpha\right)\mathbf{\Theta}_\alpha\mathbf{A}+\mathbf{\Lambda}_\beta\,\left(V^2\boldsymbol{I}-2\,\mathbf{\Lambda}_\beta\right)\mathbf{\Theta}_\beta\mathbf{B}\Big)=0. \tag{125}$$

Upon applying the operator $\hat{\mathbf{P}}_1$ on equation (115), followed by setting $r=a$ and adding the expression to the above equation results into

$$\tau^m_{rr|_{r=a}}+\tau^m_{rz|_{r=a}} = \;\hat{\mathbf{P}}_1\,\mathbf{R}_\beta\,\Big(\left(V^2\,\mathbf{I}-2\mathbf{\Lambda}_\beta\right)\mathbf{L}^T_\beta\mathbf{R}_\alpha\,\mathbf{\Lambda}_\alpha\mathbf{A}\;+\;\mathbf{\Lambda}_\beta\,\Big(V^2\mathbf{\Theta}^a_\beta-4\mathbf{\Lambda}_\beta\Big)\mathbf{B}\Big)=0. \tag{126}$$

This combination is made for mathematical ease in algebraic manipulation for dispersion analysis later on.

Applying operator $\hat{\mathbf{P}}_2$ on equation (113) and setting $r=a$ leads to

$$u^i_{r|_{r=a}} \;=\; \hat{\mathbf{P}}_2\mathbf{R}_\beta\,\Big(\mathbf{L}^T_\beta\mathbf{R}_\alpha\mathbf{Q}^V_\alpha\mathbf{\Theta}^a_\alpha\mathbf{A}-2\mathbf{\Theta}^a_\beta\mathbf{\Lambda}_\beta\mathbf{B}\Big)=0, \tag{127}$$

where

$$\mathbf{Q}^V_\alpha\equiv\frac{\mathbf{\Lambda}_\alpha\mathbf{Q}_\alpha}{k^2}=\begin{pmatrix}(V^2\;-\;\alpha^2_{\mathrm{I}}) & 0\\ 0 & (V^2\;-\;\alpha^2_{\mathrm{II}})\end{pmatrix}. \tag{128}$$

Applying operator $\hat{\mathbf{P}}_2$ on equation (116) and setting $r=a$ results into

$$\tau^i_{rz|_{r=a}} \;=\; \hat{\mathbf{P}}_2\,\mathbf{R}_\beta\,\Big(\mathbf{\Lambda}_\beta\,\mathbf{L}^T_\beta\,\mathbf{R}_\alpha\,\left(V^2\mathbf{I}-\mathbf{\Lambda}_\alpha\right)\mathbf{\Theta}_\alpha\mathbf{A}+\mathbf{\Lambda}_\beta\,\left(V^2\boldsymbol{I}-2\,\mathbf{\Lambda}_\beta\right)\mathbf{\Theta}_\beta\mathbf{B}\Big)=0. \tag{129}$$

In equations (125), (126), (127) and (129) the matrix $\mathbf{L}^T_\beta\mathbf{R}_\alpha$ describes the interaction of P and S waves. It is a coupling matrix $(\mathbf{C}_{\beta\alpha})$ defined as

$$\mathbf{L}_{\beta}^{T}\mathbf{R}_{\alpha} = \begin{bmatrix} \mathbf{l}_{\beta_I}\cdot\mathbf{r}_{\alpha_I} & \mathbf{l}_{\beta_I}\cdot\mathbf{r}_{\alpha_{II}} \\ \mathbf{l}_{\beta_{II}}\cdot\mathbf{r}_{\alpha_I} & \mathbf{l}_{\beta_{II}}\cdot\mathbf{r}_{\alpha_{II}} \end{bmatrix} \equiv \begin{bmatrix} \mathrm{C}_{\beta_I\alpha_I} & \mathrm{C}_{\beta_I\alpha_{II}} \\ \mathrm{C}_{\beta_{II}\alpha_I} & \mathrm{C}_{\beta_{II}\alpha_{II}} \end{bmatrix} \equiv \mathbf{C}_{\beta\alpha} \tag{130}$$

where $\mathrm{C}_{\beta_I\alpha_I}$ describes the interaction between the fast P wave and the fast S wave, $\mathrm{C}_{\beta_I\alpha_{II}}$ the interaction for the fast S with the slow P wave, $\mathrm{C}_{\beta_{II}\alpha_I}$ for the slow S with fast P wave and finally $\mathrm{C}_{\beta_{II}\alpha_{II}}$ for the interactions of both slow waves.

Collecting the equations (125), (126), (127) and (129) together, the linear system of equation for the constants A_I, A_{II}, B_I and B_{II} is

$$\mathbf{0} = \begin{cases} \left(V^2 - \alpha_{\mathrm{I}}^2\right) & -2\,\beta_{\mathrm{I}}^2\,\Theta_{\beta_{\mathrm{I}}}^{a}\,\hat{\boldsymbol{P}}_2\cdot\boldsymbol{r}_{\beta_{\mathrm{I}}} \\ \Theta_{\alpha_{\mathrm{I}}}^{a}\left(\hat{\boldsymbol{P}}_2\cdot\boldsymbol{r}_{\beta_{\mathrm{I}}}\mathrm{C}_{\beta_I\alpha_I} + \hat{\boldsymbol{P}}_2\cdot\boldsymbol{r}_{\beta_{\mathrm{II}}}\mathrm{C}_{\beta_{II}\alpha_I}\right) & \\ \left(V^2-\alpha_{\mathrm{I}}^2\right) & \beta_{\mathrm{I}}^2\left(V^2-2\,\beta_{\mathrm{I}}^2\right)\Theta_{\beta_{\mathrm{I}}}^{a}\,\boldsymbol{P}_1\cdot\boldsymbol{r}_{\beta_{\mathrm{I}}} \\ \Theta_{\alpha_{\mathrm{I}}}^{a}\left(\beta_{\mathrm{I}}^2\hat{\boldsymbol{P}}_1\cdot\boldsymbol{r}_{\beta_{\mathrm{I}}}\mathrm{C}_{\beta_I\alpha_I} + \beta_{\mathrm{II}}^2\hat{\boldsymbol{P}}_1\cdot\boldsymbol{r}_{\beta_{\mathrm{II}}}\mathrm{C}_{\beta_{II}\alpha_I}\right) & \\ \left(V^2-\alpha_{\mathrm{I}}^2\right) & \beta_{\mathrm{I}}^2\left(V^2-2\,\beta_{\mathrm{I}}^2\right)\Theta_{\beta_{\mathrm{I}}}^{a}\,\hat{\boldsymbol{P}}_2\cdot\boldsymbol{r}_{\beta_{\mathrm{I}}} \\ \Theta_{\alpha_{\mathrm{I}}}^{a}\left(\beta_{\mathrm{I}}^2\hat{\boldsymbol{P}}_2\cdot\boldsymbol{r}_{\beta_{\mathrm{I}}}\mathrm{C}_{\beta_I\alpha_I} + \beta_{\mathrm{II}}^2\hat{\boldsymbol{P}}_2\cdot\boldsymbol{r}_{\beta_{\mathrm{II}}}\mathrm{C}_{\beta_{II}\alpha_I}\right) & \\ \alpha_{\mathrm{I}}^2\left\{(V^2-2\beta_{\mathrm{I}}^2)\hat{\boldsymbol{P}}_1\cdot\boldsymbol{r}_{\beta_{\mathrm{I}}}\mathrm{C}_{\beta_I\alpha_I} + \right. & \beta_I^2\left(V^2\,\Theta_{\beta_I}^{a} - 4\beta_I^2\right)\hat{\boldsymbol{P}}_1\cdot\mathbf{r}_{\beta_I} \\ \left.(V^2-2\beta_{\mathrm{II}}^2)\hat{\boldsymbol{P}}_1\cdot\boldsymbol{r}_{\beta_{\mathrm{II}}}\mathrm{C}_{\beta_{II}\alpha_I}\right\} & \end{cases}$$

$$
\begin{pmatrix}
\left(V^2-\alpha_{\text{II}}^2\right) & -2\beta_{\text{II}}^2\,\Theta^a_{\beta_{\text{II}}}\hat{\boldsymbol{P}}_2\cdot\boldsymbol{r}_{\beta_{\text{II}}} \\
\Theta^a_{\alpha_{\text{II}}}\left(\hat{\boldsymbol{P}}_2\cdot\boldsymbol{r}_{\beta_{\text{I}}}\mathrm{C}_{\beta_I\alpha_{II}}+\hat{\boldsymbol{P}}_2\cdot\boldsymbol{r}_{\beta_{\text{II}}}\mathrm{C}_{\beta_{II}\alpha_{II}}\right) & \\
\left(V^2-\alpha_{\text{II}}^2\right) & \beta_{\text{II}}^2\,\left(V^2-2\,\beta_{\text{II}}^2\right)\,\Theta^a_{\beta_{\text{II}}}\hat{\boldsymbol{P}}_1\cdot\boldsymbol{r}_{\beta_{\text{II}}} \\
\Theta^a_{\alpha_{\text{II}}}\left(\beta_{\text{I}}^2\hat{\boldsymbol{P}}_1\cdot\boldsymbol{r}_{\beta_{\text{I}}}\mathrm{C}_{\beta_I\alpha_{II}}+\beta_{\text{II}}^2\hat{\boldsymbol{P}}_1\cdot\boldsymbol{r}_{\beta_{\text{II}}}\mathrm{C}_{\beta_{II}\alpha_{II}}\right) & \\
\left(V^2-\alpha_{\text{II}}^2\right) & \beta_{\text{II}}^2\,\left(V^2-2\,\beta_{\text{II}}^2\right)\,\Theta^a_{\beta_{\text{II}}}\hat{\boldsymbol{P}}_2\cdot\boldsymbol{r}_{\beta_{\text{II}}} \\
\Theta^a_{\alpha_{\text{II}}}\left(\beta_{\text{I}}^2\hat{\boldsymbol{P}}_2\cdot\boldsymbol{r}_{\beta_{\text{I}}}\mathrm{C}_{\beta_I\alpha_{II}}+\beta_{\text{II}}^2\hat{\boldsymbol{P}}_2\cdot\boldsymbol{r}_{\beta_{\text{II}}}\mathrm{C}_{\beta_{II}\alpha_{II}}\right) & \\
\alpha_{\text{II}}^2\left\{(V^2-2\beta_{\text{I}}^2)\hat{\boldsymbol{P}}_1\cdot\boldsymbol{r}_{\beta_{\text{I}}}\mathrm{C}_{\beta_I\alpha_{II}}+\right. & \beta_{II}^2\left(V^2\,\Theta^a_{\beta_{II}}-4\beta_{II}^2\right)\,\hat{\mathbf{P}}_1\cdot\mathbf{r}_{\beta_{II}} \\
\left.(V^2-2\beta_{\text{II}}^2)\hat{\boldsymbol{P}}_1\cdot\boldsymbol{r}_{\beta_{\text{II}}}\mathrm{C}_{\beta_{II}\alpha_{II}}\right\} &
\end{pmatrix}
\begin{pmatrix} A_I \\ B_I \\ A_{II} \\ B_{II} \end{pmatrix} \tag{131}
$$

where equations for vanishing u_r^i, τ_{rz}^m, τ_{rz}^i and $(\tau_{rr}^m+\tau_{rz}^m)$ correspond to the first, second, third and fourth row, respectively. This system of equations define the modes of longitudinal vibration in a porous cylinder with stress-free impermeable radial surface.

4.6 Dispersion polynomial

The non-trivial solution of the system of equations (131) is obtained by setting the determinant of its 4×4 coefficient matrix equal to zero. The vanishing determinant of this matrix yields a polynomial which describes the behavior of waves under the applied boundary conditions and it is the dispersion relation. The determinant, which was computed using Wolfram Mathematica, is a third order polynomial[2] in V^2 as below

$$B_3Z^3+B_2Z^2+B_1Z+B_0=0, \tag{132}$$

where $Z=V^2$ and coefficients are

[2]There is an additional trivial root of V^2 which is ignored.

$$B_0 = 4\alpha_{\rm I}\,\alpha_{\rm II}\,\beta_{\rm mi} \left\{(\beta_{\rm I}-\beta_{\rm II})(h_1\,h_2\,\Theta^a_{\alpha_{\rm I}} - h_3\,h_4\,\Theta^a_{\alpha_{\rm II}})\,\Theta^a_{\beta_{\rm I}}\,\Theta^a_{\beta_{\rm II}} + \alpha_{\rm mi}\,h_5\,(\alpha_{\rm I}-\alpha_{\rm II})\,\Theta^a_{\alpha_{\rm I}}\,\Theta^a_{\alpha_{\rm II}}\right\} \quad (133)$$

$$B_1 = 4\left(\alpha^2_{\rm II}-\alpha^2_{\rm I}\right)\alpha_{\rm mi}\beta_{\rm mi}\Theta^a_{\alpha_{\rm I}}\Theta^a_{\alpha_{\rm II}} - \left(\beta_{\rm I}-\beta_{\rm II}\right)\Big\{2\alpha_{\rm II}\left(2h_1h_6\beta_{\rm mi}+(h_7+h_9-\alpha_{\rm I}\beta_{\rm mi}h_1)\right)\Theta^a_{\alpha_{\rm I}} -2\alpha_{\rm I}\left(2h_3h_6\beta_{\rm mi}+\alpha_{\rm II}\left(h_7+h_8-\alpha_{\rm II}\beta_{\rm mi}h_3\right)\right)\Theta^a_{\alpha_{\rm II}} + \alpha_{\rm I}\alpha_{\rm II}\alpha_{\rm mi}\beta_{\rm mi}\beta_{\rm mm}h_{14}\Big\}\Theta^a_{\beta_{\rm I}}\Theta^a_{\beta_{\rm II}} \quad (134)$$

$$B_2 = (\alpha_{\rm I}-\alpha_{\rm II})\,\alpha_{\rm mi}\,\beta_{\rm mi}\,\Theta^a_{\alpha_{\rm I}}\Theta^a_{\alpha_{\rm II}}\left[4h_5+(\alpha_{\rm I}+\alpha_{\rm II})\left(\beta_{\rm I}-\beta_{\rm II}\right)\beta_{\rm mm}\,\Theta^a_{\beta_{\rm I}}\Theta^a_{\beta_{\rm II}}\right] + (2\,h_{10}+h_{12})\,\alpha_{\rm I}\left(\beta_{\rm I}-\beta_{\rm II}\right)\Theta^a_{\alpha_{\rm II}}\Theta^a_{\beta_{\rm I}}\Theta^a_{\beta_{\rm II}} - (2\,h_{10}+h_{11})\,\alpha_{\rm II}\left(\beta_{\rm I}-\beta_{\rm II}\right)\Theta_{\alpha_{\rm I}}\Theta^a_{\beta_{\rm I}}\Theta^a_{\beta_{\rm II}} \quad (135)$$

$$B_3 = \alpha_{\rm mi}\left(\beta_{\rm I}-\beta_{\rm II}\right)\beta_{\rm mi}\,\left\{h_{13}-(\alpha_{\rm I}+\alpha_{\rm II})\,\beta_{\rm mm}\,\Theta^a_{\alpha_{\rm I}}\Theta^a_{\alpha_{\rm II}}\right\}\Theta^a_{\beta_{\rm I}}\Theta^a_{\beta_{\rm II}} \quad (136)$$

with

$$h_1 = ((\alpha_{\rm II}-\alpha_{\rm mm})\,\beta_{\rm mi}+\alpha_{\rm mi}\,\beta_{\rm mm}) \quad (137)$$

$$h_2 = (\alpha_{\rm mi}\,\beta_{\rm im}-(\alpha_{\rm I}-\alpha_{\rm mm})\,\beta_{\rm mm}) \quad (138)$$

$$h_3 = ((\alpha_{\rm I}-\alpha_{\rm mm})\,\beta_{\rm mi}+\alpha_{\rm mi}\,\beta_{\rm mm}) \quad (139)$$

$$h_4 = (\alpha_{\rm mi}\,\beta_{\rm im}-(\alpha_{\rm II}-\alpha_{\rm mm})\,\beta_{\rm mm}) \quad (140)$$

$$h_5 = \beta^2_{\rm II}\left(\beta_{\rm I}-\beta_{\rm mm}\right)\Theta^a_{\beta_{\rm I}} - \beta^2_{\rm I}\left(\beta_{\rm II}-\beta_{\rm mm}\right)\Theta^a_{\beta_{\rm II}} \quad (141)$$

$$h_6 = \alpha_{\rm mi}\,\beta_{\rm im}-\alpha_{\rm mm}\,\beta_{\rm mm} \quad (142)$$

$$h_7 = 2\,\alpha_{\rm mi}\,\beta_{\rm mi}\,(\alpha_{\rm mm}-\beta_{\rm mm})\,\beta_{\rm mm}-{\alpha_{\rm mi}}^2\left(\beta_{\rm I}-\beta_{\rm mm}\right)\left(\beta_{\rm II}-\beta_{\rm mm}\right) \quad (143)$$

$$h_8 = {\beta_{\rm mi}}^2\,(\alpha_{\rm I}-\alpha_{\rm mm})\,(\alpha_{\rm mm}-2\,\beta_{\rm mm}) \quad (144)$$

$$h_9 = {\beta_{\rm mi}}^2\,(\alpha_{\rm II}-\alpha_{\rm mm})\,(\alpha_{\rm mm}-2\,\beta_{\rm mm}) \quad (145)$$

$$h_{10} = {\beta_{\rm mi}}^2\,(\alpha_{\rm I}-\alpha_{\rm mm})\,(\alpha_{\rm II}-\alpha_{\rm mm})+{\alpha_{\rm mi}}^2\left(\beta_{\rm I}-\beta_{\rm mm}\right)\left(\beta_{\rm II}-\beta_{\rm mm}\right) \quad (146)$$

$$h_{11} = \alpha_{\rm mi}\,\beta_{\rm mi}\,(\alpha_{\rm I}-\alpha_{\rm mm})\,(\alpha_{\rm I}+4\,\beta_{\rm mm}) \quad (147)$$

$$h_{12} = \alpha_{\rm mi}\,\beta_{\rm mi}\,(\alpha_{\rm II}-\alpha_{\rm mm})\,(\alpha_{\rm I}+4\,\beta_{\rm mm}) \quad (148)$$

$$h_{13} = \alpha_{\rm II}\,(\alpha_{\rm I}-\alpha_{\rm mm})\,\Theta^a_{\alpha_{\rm I}}-\alpha_{\rm I}\,(\alpha_{\rm II}-\alpha_{\rm mm})\,\Theta^a_{\alpha_{\rm II}} \quad (149)$$

$$h_{14} = \alpha_{\rm I}\left(\Theta^a_{\alpha_{\rm II}}-2\right)\Theta^a_{\alpha_{\rm I}}-\alpha_{\rm II}\left(\Theta^a_{\alpha_{\rm I}}-2\right)\Theta^a_{\alpha_{\rm II}} \quad (150)$$

Chapter 5 Dispersion relation for extensional waves

The extensional waves are a particular case of the longitudinal motion wherein the axial motion is compressional in nature, that is, the direction of propagation is along the axial direction, and the radial motion is shear in nature. Such oscillation is excited when a non-vanishing component of stress is in axial direction only and the wavelength is orders in magnitude greater than radius of the cylinder. In contrast to the elastic case, for the poroelastic case, there are more than one such mode because a porous medium supports two compressional and two shear waves.

In this chapter, the slender rod approximation of longitudinal solution is derived. That is, the extensional limit case is developed for which the ratio of radius to wavelength is less than one. The approximations for the transcendental functions Θ_α and Θ_β are derived in §5.1. Thereafter, in §5.2 the companion matrix technique is utilized to find the roots of the dispersion relation. This method solves for roots of a polynomial by constructing a (companion) matrix with the characteristic equation that is the same as the polynomial in question. In this manner, solving for roots is reduced to solving an eigenvalue problem. In §5.3 for illustrative purposes the numerical computation of the dispersion relation is carried out with physical properties of a sample of Berea sandstone.

5.1 Approximations of theta functions

The longitudinal dispersion relation (132) involves Θ functions, which are the ratio of Bessel functions as $2\frac{J_1(z)}{zJ_0(z)}$. For the limiting case of small and large arguments exist algebraic approximations for the Θ function (Solorza and Sahay, 2009). Those approximations are

$$\Theta(z) \approx \begin{cases} 1 + \frac{1}{8}z^2 - \frac{1}{24}z^4 + ... & \text{for} \quad z < 1 \\ \frac{2}{z} & \text{for} \quad z > 1. \end{cases} \tag{151}$$

5.1.1 Theta functions for the fast-P and fast-S waves

For the case of the fast-P wave, the argument of $\Theta^a_{\alpha_{\mathrm{I}}}(z)$ is

$$z = aq_{\alpha_I} = a\sqrt{\frac{\omega^2}{\alpha_I^2} - k^2} = a\sqrt{\omega^2\left(\frac{1}{\alpha_I^2} - \frac{k^2}{\omega^2}\right)} = a\omega\sqrt{\frac{1}{\alpha_I^2} - \frac{1}{V^2}}. \tag{152}$$

Therefore, in the low frequency regime, $aq_{\alpha_I} < 1$, $\Theta^a_{\alpha_{\rm I}}$ is approximated as

$$\Theta^a_{\alpha_{\rm I}} = \Theta^a_{\alpha_{\rm I}}(aq_{\alpha_I}) \approx 1 + \frac{a^2\omega^2}{8}\left(\frac{1}{\alpha_I^2} - \frac{1}{V^2}\right). \tag{153}$$

For common geomaterials in the low frequency regime, $\|\frac{a^2\omega^2}{8}\left(\frac{1}{\alpha_I^2} - \frac{1}{V^2}\right)\| \ll 1$, so one may take in such cases

$$\Theta^a_{\alpha_{\rm I}}(aq_{\alpha_I}) \approx 1\,. \tag{154}$$

Similarly, for the fast-S wave, the argument of $\Theta^a_{\beta_{\rm I}}(z)$ is

$$z = aq_{\beta_I} = a\sqrt{\frac{\omega^2}{\beta_I^2} - k^2} = a\sqrt{\omega^2\left(\frac{1}{\beta_I^2} - \frac{k^2}{\omega^2}\right)} = a\omega\sqrt{\frac{1}{\beta_I^2} - \frac{1}{V^2}}, \tag{155}$$

which is less than 1 for low frequency regime. So $\Theta^a_{\beta_{\rm I}}$ is approximated as

$$\Theta^a_{\beta_{\rm I}} = \Theta^a_{\beta_{\rm I}}(aq_{\beta_I}) \approx 1 + \frac{a^2\omega^2}{8}\left(\frac{1}{\beta_I^2} - \frac{1}{V^2}\right) \approx 1. \tag{156}$$

5.1.2 Theta functions for the slow-P and slow-S waves

For the case of slow-P wave, the argument of $\Theta^a_{\alpha_{\rm II}}$ is approximated as

$$z = aq_{\alpha_{II}} = a\sqrt{\frac{\omega^2}{\alpha_{II}^2} - k^2} = a\sqrt{\frac{\omega^2}{\alpha_{II}^2}\left(1 - \frac{\alpha_{II}^2}{V^2}\right)} \approx a\frac{\omega}{\alpha_{II}}\left(1 - \frac{1}{2}\frac{\alpha_{II}^2}{V^2}\right) \tag{157}$$

where $|\frac{\alpha_{II}}{V}| \ll 1$ in the low frequency regime, so

$$aq_{\alpha_{II}} \approx a\frac{\omega}{\alpha_{II}}. \tag{158}$$

For frequencies below the Biot relaxation frequency, the norm $|\alpha_{\rm II}| \ll 1$ implies that $aq_{\alpha_{II}} > 1$. So, $\Theta^a_{\alpha_{\rm II}}$ is approximated as

$$\Theta^a_{\alpha_{\rm II}}(aq_{\alpha_{II}}) \approx 2\frac{\alpha_{II}}{a\,\omega}. \tag{159}$$

In the same manner, for the slow-S wave, the argument of $\Theta^a_{\beta_{\rm II}}(z)$ is approximated as

$$z = aq_{\beta_{II}} = a\sqrt{\frac{\omega^2}{\beta_{II}^2}\left(1 - \frac{\beta_{II}^2}{V^2}\right)} \approx a\frac{\omega}{\beta_{II}}\left(1 - \frac{1}{2}\frac{\beta_{II}^2}{V^2}\right) \approx a\frac{\omega}{\beta_{II}}, \tag{160}$$

where $a\frac{\omega}{\beta_{II}} \gg 1$ in the low frequency regime. So, $\Theta^a_{\beta_{\rm II}}$ becomes

$$\Theta^a_{\beta_{\rm II}} = \Theta^a(aq_{\beta_{II}}) \approx 2\frac{\beta_{II}}{a\,\omega}. \tag{161}$$

5.2 Companion matrix technique

The companion matrix technique is a powerful tool to solve a polynomial of high order. It solves for roots of a polynomial by computing the eigenvalues of the matrix that has the polynomial in question as its characteristic equation (Golub and Van Loan, 1996; section 7.4.6).

The dispersion polynomial (132), after rescaling with respect to its leading term coefficient is

$$z^3 + a_2 z^2 + a_1 z + a_0 = 0 \tag{162}$$

where $a_0 = \frac{B_0}{B_3}$, $a_1 = \frac{B_1}{B_3}$ and $a_2 = \frac{B_2}{B_3}$.

The solution of (162) is computed by solving the eigenvalue problem of the matrix $\boldsymbol{M}$ of the following structure

$$\boldsymbol{M} = \begin{pmatrix} 0 & 0 & -a_0 \\ 1 & 0 & -a_1 \\ 0 & 1 & -a_2 \end{pmatrix} \tag{163}$$

where the roots of dispersion relation (162) are the eigenvalues of $\boldsymbol{M}$.

5.3 Numerical solution of the dispersion relation

The dispersion relation (162) is solved by the companion matrix technique. In order to probe for the behavior of a real geo-material, the numerical solution of the dispersion relation is computed with physical properties of a sample of Berea sandstone saturated with water. The data of physical properties are presented in Table 6. The solution of the dispersion relation is computed for the regime below the Biot critical frequency, which for this case is 2.04×10^7 Hz. This solution exhibits that there exists three natural modes of extensional motion.

Table 6: Physical properties of water saturated Berea sandstone

fluid density:	$\rho_{\mathrm{f}}^{0} = 1.00 \times 10^{+03}\left(\frac{kg}{m^3}\right)$
fluid bulk modulus:	$\mathrm{K_f} = 2.2 \times 10^{+09}\,(Pa)$
fluid bulk viscosity:	$\xi_{\mathrm{f}} = 2.8 \times 10^{-03}\left(\frac{kg}{m^3}\right)$
fluid shear viscosity:	$\mu_{\mathrm{f}} = 1.00 \times 10^{-03}\left(\frac{kg}{m^3}\right)$
solid density:	$\rho_{\mathrm{s}}^{0} = 2.65 \times 10^{+03}\left(\frac{kg}{m^3}\right)$
solid-mineral shear modulus:	$\mu_{\mathrm{s}} = 2.30 \times 10^{+10}\,(Pa)$
solid-frame shear modulus:	$\mu_{_0} = 6.70 \times 10^{+09}\,(Pa)$
solid-frame bulk modulus:	$\mathrm{K}_0 = 5.20 \times 10^{+09}\,(Pa)$
solid-mineral bulk modulus:	$\mathrm{K_s} = 35 \times 10^{+09}\,(Pa)$
permeability:	$K = 1.00 \times 10^{-14}\,(m^2)$
porosity:	$\eta_{_0} = 0.25$
tortuosity factor:	$\mathrm{S} = \frac{4}{3}$
radius of the cylindrical core:	$a = 1.9 \times 10^{-2}\,(m)$

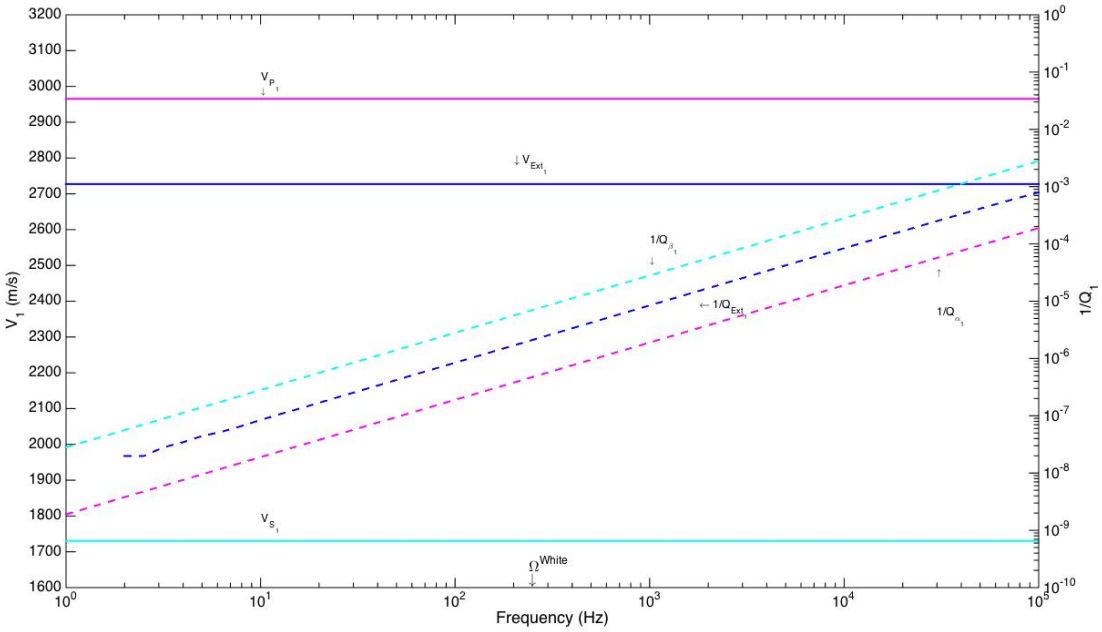

Figure 1: Dispersion curve for the first extensional mode. The phase velocity (solid-line) and attenuation (dash-line) of the extensional mode are shown in blue. For reference purposes, the fast-P and fast-S phase velocities (solid-line) and attenuation (dash-line) are presented in magenta and cyan, respectively.

The first mode describes a wave with the velocity in between fast-P and fast-S velocities. For the low regime, this mode has insignificant attenuation, although it is linearly increasing with frequency. In Figure (1), the phase velocity of this mode is represented by the blue solid-line and its attenuation

represented by the blue dash-line. For reference purposes, the phase velocities (solid line) and attenuation (dash-line) of the fast-P and fast-S waves are plotted in the colors magenta and cyan, respectively.

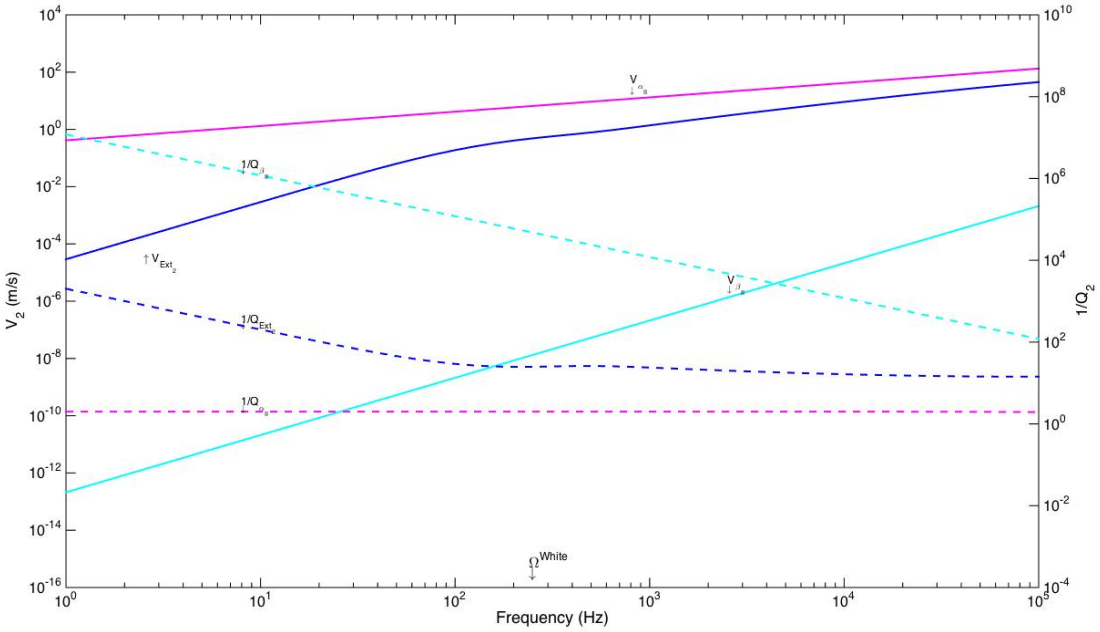

Figure 2: Dispersion curve for the second extensional mode. The phase velocity (solid-line) and attenuation (dash-line) of the extensional mode are shown in blue. For reference purposes, the slow-P and slow-S phase velocities (solid-line) and attenuations (dash-line) are presented in magenta and cyan, respectively.

In Figure (2), the second extensional mode (blue lines) is presented together with the slow-P (megenta) and slow-S (cyan) waves. Also, the frequency for which the slow-P wavelength is equal to the sample radius, the White frequency (White, 1986), is marked. The nature of this mode changes at the White frequency, which in this case is 239 Hz. It is apparent that this mode is due to the interaction of the slow-P and slow-S motions. In the regime below the White frequency, the mode is strongly influenced by slow-S wave. In the regime above the White frequency, its nature is dominated by slow-P wave, however, significantly more dampened than slow-P wave.

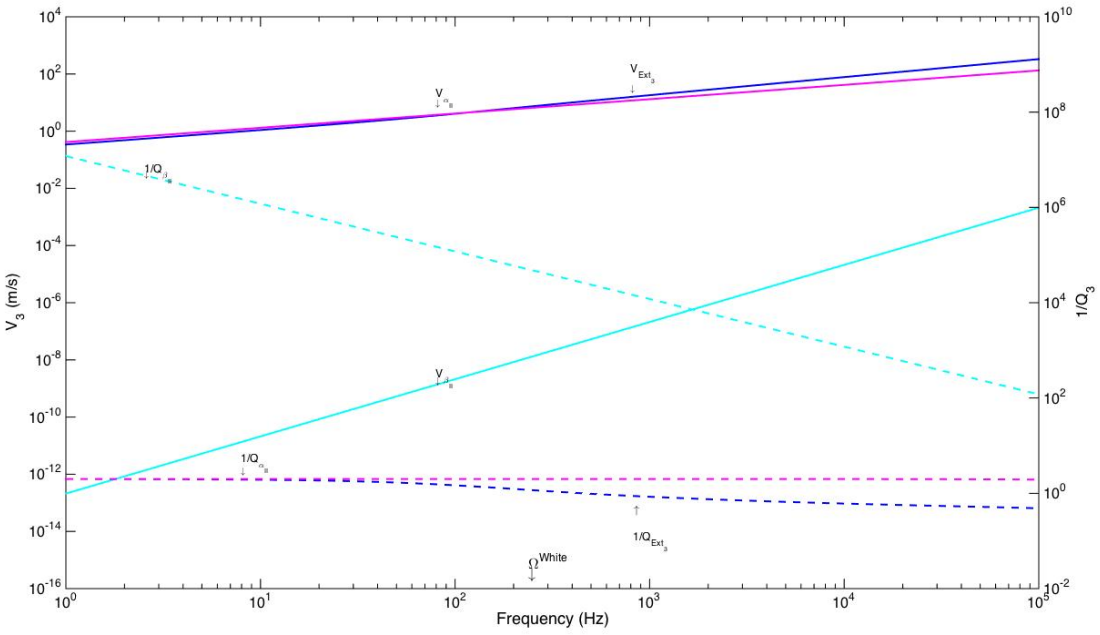

Figure 3: Dispersion curve for the third extensional mode. The phase velocity (solid-line) and attenuation (dash-line) of the extensional mode are shown in blue. For reference purposes, the slow-P and slow-S phase velocities (solid-line) and attenuations (dash-line) are presented in magenta and cyan, respectively.

The third mode is plotted in the Figure (3) with slow-P (red) and slow-S (blue) waves for reference purposes. This mode is a slow-P wave. It is progressively faster and less attenuating in the frequency regime above the White frequency, although still remains diffusive in character. Below the White frequency, it is essentially a slow-P wave.

Chapter 6 Analysis of the nature of waves

The numerical solution of the dispersion relation shows the existence of three extensional modes for a saturated porous cylinder with stress-free impermeable radial surface with each mode having a characteristic behavior. In order to interpret the LF measurements, it is necessary to understand the nature of these modes. The LF experiments are the studies of sub-resonance extensional motion of porous cylindrical cores that have non-vanishing stresses at its impermeable radial surface. Therefore, the observed motion in a LF experiment is naturally a combination of these three modes of the stress-free impermeable case.

Furthermore, these modes ought to be related with the modes generated when the fluid is able to move through the radial surface that is stress-free, the stress-free open-pore case, which are fully understood (Gardner, 1962; Berryman, 1983; White, 1986; Dunn, 1986; Johnson and Kostek, 1995; Solorza and Sahay, 2009).

A synthesis of the stress-free open-pore extensional mode problem is presented in Solorza and Sahay (2009), who have analyzed in the dCS framework and shown the existence of three natural modes. Therein, the first mode is the coupled fast-P and fast-S waves. Below White's frequency it tends to become the extensional motion of the drained frame only, and in the regime above White frequency, it is the extensional motion of the undrained frame, i.e., the effective Gassmann elastic solid. There is an attenuation peak, at the White frequency, due to the in and out fluid flow through open pore at the radial surface. Here, both second and third modes are the manifestations of interacting slow-P and slow-S processes, which respectively degenerate to slow-P and slow-S waves in the regime above the Biot critical frequency. These two modes are damped so heavily that energy pumped into these modes dies off rapidly.

In this chapter the nature of each of the three closed-pore modes are analyzed and compared with the modes that occur in open-pore case (§6.1, §6.2, §6.3). Then, in section §6.4, the velocity and attenuation of the first extensional mode is expressed in terms of physical properties by carrying out an asymptotic approximation.

6.1 First extensional mode with stress-free impermeable radial surface

The first extensional mode in a porous cylinder with impermeable radial surface is coupled fast-P and fast-S motion. The velocity of this mode corresponds to the extensional modulus of the undrained frame, i.e., an effective undrained elastic solid (Gassmann medium). While the attenuation, although not significant, is linear dependent on frequency.

Due to the impermeable surface, the fluid is not capable to relax the pressure through the radial surface, so there is no attenuation peak at the White frequency, as it occurs in the open-pore case. This is illustrated in Figure (4). Also, in closed-pore case there is no longer dry-frame (or drained) behavior. So, for all frequencies below the Biot critical frequency the velocity corresponds to that of the extensional modulus of the effective (undrained) elastic medium.

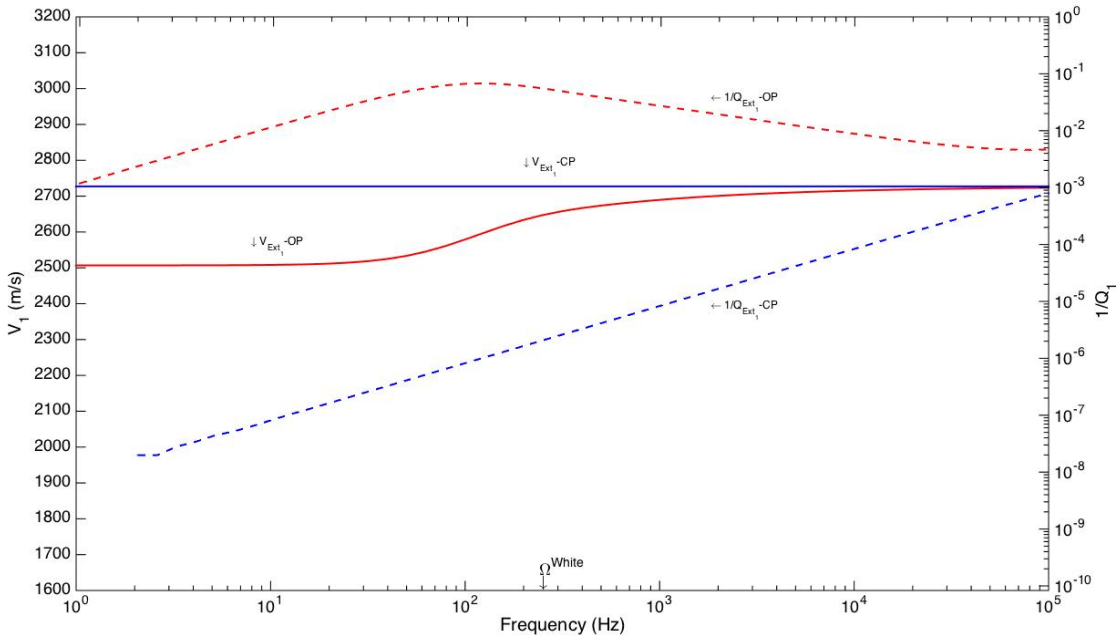

Figure 4: Comparison of the first extensional modes of the closed-pore (CP) and open-pore (OP) cases. The phase velocity (solid-line) and attenuation (dash-line) for the closed-pore and open-pore cases are shown in blue and red, respectively.

6.2 Second extensional mode with stress-free impermeable radial surface

The second extensional mode is a diffusion process. It is due to the interactions of the slow-P and slow-S waves. Its velocity is in between those two waves and it can be interpreted as a slow-extensional wave. This mode is highly attenuated and its attenuation is the largest among the three extensional modes. The attenuation is so high that it dampens within a minuscule fraction of a cycle.

By comparing this mode with the second and third extensional modes generated in the open pore case Figure (4), one finds it to be a combination of the two open pore cases. This phenomenon could be attributed to the influence of the impermeable radial surface.

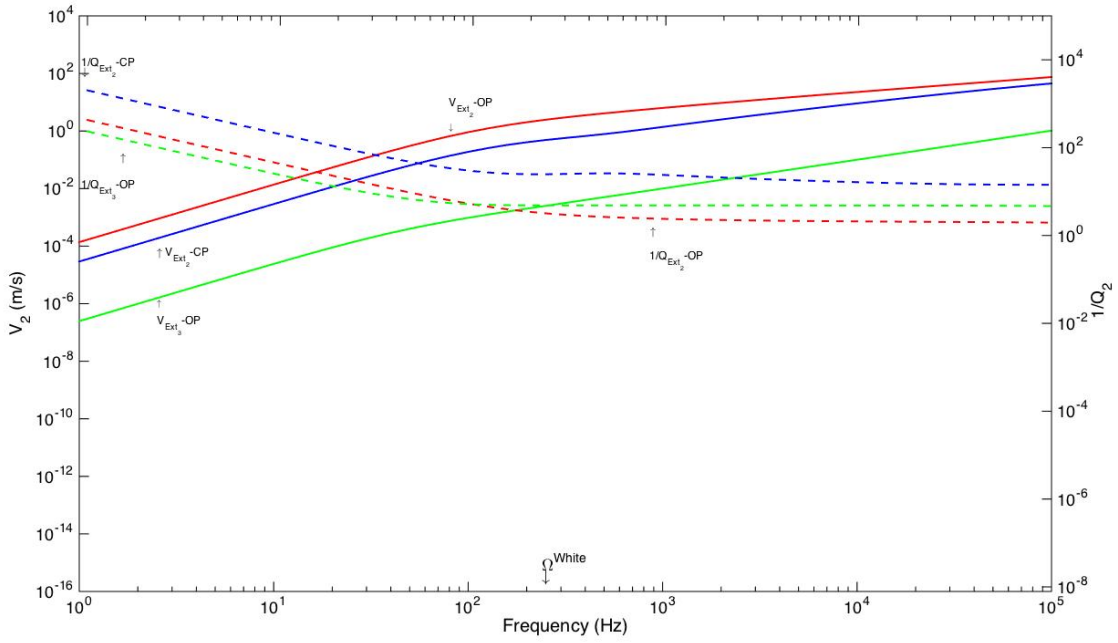

Figure 5: Comparisons of the second mode of the closed-pore (CP) and with the second and third extensional modes of the open-pore (OP) case. The phase velocity (solid-line) and inverse (dash-line) of closed pore case are shown in blue. The phase velocity (solid-line) and attenuation (dash-line) of the second and third modes of the open-pore case are plotted in red and green, respectively.

6.3 Third extensional mode with stress-free impermeable radial surface

The third extensional mode for closed-pore case behaves as a slow-P wave. It is a diffusive process and its velocity and attenuation are close to the slow-P wave. Unlike the second and third modes of the open-pore case, this mode is not influenced by the slow-S process at all. Its existence as a pure slow P-wave is due to the impermeable radial surface.

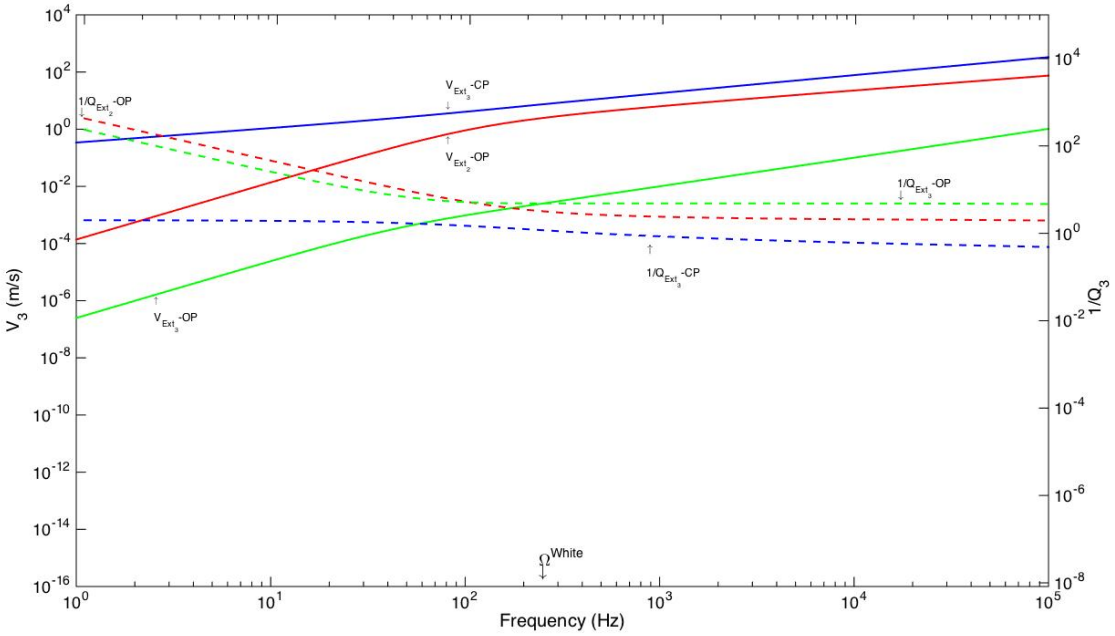

Figure 6: Comparisons for the third extensional mode of the closed-pore (CP) case and the second and third extensional modes of the open-pore (OP) case. The phase velocity (solid-line) and inverse attenuation (dash-line) of closed pore case are shown in blue. The phase velocity (solid-line) and inverse attenuation (dash-line) of the second and third modes of the open-pore case are plotted in red and green, respectively.

6.4 Asymptotic approximation of the first extensional mode

In order to relate the first extensional mode velocity and its attenuation with physical properties, their analytical expressions are developed using the exact formula for roots of a third order polynomial. Thereafter, the leading parts from their analytical expressions are extracted out to the extent needed to match the exact values in the desired domain.

The exact solution of the third order dispersion relation (132) is written, using the formula given by Press et al. (1996), as

$$Z_1 = A + B - \frac{B_2}{3B_3}, \tag{164}$$

$$Z_2 = -\frac{1}{2}(A+B) - \frac{B_2}{3B_3} + \mathbf{i}\frac{\sqrt{3}}{2}(A-B), \tag{165}$$

$$Z_3 = -\frac{1}{2}(A+B) - \frac{B_2}{3B_3} - \mathbf{i}\frac{\sqrt{3}}{2}(A-B), \tag{166}$$

with,

$$A = \left(R + \sqrt{R^2 - T^3}\right)^{\frac{1}{3}}, \tag{167}$$

$$B = \begin{cases} \frac{T}{A} & \text{if} \quad A \neq 0 \\ 0 & \text{if} \quad A = 0 \end{cases}, \tag{168}$$

$$T = \frac{(\frac{B_2}{B_3})^2 - 3\frac{B_1}{B_3}}{9}, \tag{169}$$

$$R = \frac{2(\frac{B_2}{B_3})^3 - 9\frac{B_1 B_2}{(B_3)^2} + 27\frac{B_0}{B_3}}{54}, \tag{170}$$

where B_0, B_1, B_2 and B_3 are the coefficients of the dispersion polynomial (132).

The approximations for the elements of matrices $\boldsymbol{\alpha}$ and $\boldsymbol{\beta}$ below the Biot critical frequency are developed by Solorza and Sahay (2009) for micro-homogeneous case. Extending those to include the micro-inhomogeneous term, the expressions become

$$\alpha_{\mathrm{mm}} \approx \alpha_{\mathrm{c}}^{\star 2}, \tag{171}$$

$$\alpha_{\mathrm{mi}} \approx \alpha_{\mathrm{c}}^{\star 2}\frac{m_{\mathrm{f}}}{\mathrm{m_d}}\left(1 - \frac{\alpha^\star}{\eta_0}\frac{\alpha_{\mathrm{fl}}^{\star 2}}{\alpha_{\mathrm{c}}^{\star 2}}\right), \tag{172}$$

$$\alpha_{\mathrm{im}} \approx \alpha_{\mathrm{c}}^{\star 2}\mathrm{d_f}\left(\left(\frac{\omega}{\Omega_{\mathrm{i}}}\right)^2 - i\left(\frac{\omega}{\Omega_{\mathrm{i}}}\right)\right)\left(1 - \frac{\alpha}{\eta_0}\frac{\alpha_{\mathrm{fl}}^{\star 2}}{\alpha_{\mathrm{c}}^{\star 2}}\right)\mathrm{m_d}, \tag{173}$$

$$\alpha_{\mathrm{ii}} \approx \alpha_{\mathrm{c}}^{\star 2}\mathrm{d_f}\left(\left(\frac{\omega}{\Omega_{\mathrm{i}}}\right)^2 - i\left(\frac{\omega}{\Omega_{\mathrm{i}}}\right)\right)(\mathrm{m_f} + \varepsilon^\star), \tag{174}$$

and

$$\beta_{\mathrm{mm}} = \beta_{\mathrm{c}}^2\left(1 - i\frac{\omega}{\Omega_\beta}\alpha_{_\mu}\right), \tag{175}$$

$$\beta_{\mathrm{mi}} = \beta_{\mathrm{c}}^2\left(1 + i\frac{\omega}{\Omega_\beta}\left(\frac{\eta_0}{\mathrm{m_f}} - \alpha_{_\mu}\right)\right)\frac{\mathrm{m_f}}{\mathrm{m_d}}, \tag{176}$$

$$\beta_{\mathrm{im}} \approx \beta_{\mathrm{c}}^2\left[\left(\frac{\omega}{\Omega_{\mathrm{i}}}\right)^2 - i\left(\frac{\omega}{\Omega_{\mathrm{i}}}\right)\right]\left(\mathrm{d_f} + i\frac{\omega}{\Omega_\beta}\mathrm{d_s}\alpha_{_\mu}\right)\mathrm{m_d}, \tag{177}$$

$$\beta_{\mathrm{ii}} \approx \beta_{\mathrm{c}}^2\left[\left(\frac{\omega}{\Omega_{\mathrm{i}}}\right)^2 - i\left(\frac{\omega}{\Omega_{\mathrm{i}}}\right)\right]\left(\mathrm{d_f} - i\frac{\omega}{\Omega_\beta}\mathrm{d_s}\left(\frac{\eta_0}{\mathrm{m_f}} - \alpha_{_\mu}\right)\right)\mathrm{m_f}. \tag{178}$$

Furthermore, in the region below Biot critical frequency, the complex square fast- and slow- P velocities are

$$\alpha_{\mathrm{I}}^2 \approx \alpha_{\mathrm{c}}^{\star 2}\left[1 - i\left(\frac{\omega}{\Omega_{\mathrm{i}}}\right)\left\{\mathrm{d_f m_f}\left(1 - \frac{\alpha^\star}{\eta_0}\frac{\alpha_{\mathrm{fl}}^{\star 2}}{\alpha_{\mathrm{c}}^{\star 2}}\right)\left(1 - \frac{\alpha}{\eta_0}\frac{\alpha_{\mathrm{fl}}^{\star 2}}{\alpha_{\mathrm{c}}^{\star 2}}\right)\right\}\right], \tag{179}$$

$$\alpha_{\mathrm{II}}^2 \approx \left\{\mathrm{d_f}\alpha_{\mathrm{fl}}^{\star 2}\frac{\mathrm{H_0}}{\mathrm{H_c}}\right\}\left[\left(\frac{\omega}{\Omega_{\mathrm{i}}}\right)^2\left(1 + \mathrm{d_f}\left(\mathrm{m_f} + \varepsilon^\star\right)\right) - i\left(\frac{\omega}{\Omega_{\mathrm{i}}}\right)\right], \tag{180}$$

and, the fast- and slow- S velocities are

$$\beta_{\mathrm{I}}^2 \approx \beta_{\mathrm{c}}^2\left(1 - i\left(\frac{\omega}{\Omega_{\mathrm{i}}}\right)\mathrm{d_f m_f}\right), \tag{181}$$

$$\beta_{\mathrm{II}}^2 \approx -\omega\left(\frac{\omega}{\Omega_{\mathrm{i}}}\right)\left[1 + i\left(\frac{\omega}{\Omega_{\mathrm{i}}}\right)\left(1 + \mathrm{d_f m_f}\right)\right]\mathrm{d_f}\nu_{\mathrm{f}}. \tag{182}$$

By applying the approximations (171)−(182), as well as $\Theta^a_{\alpha_{\mathrm{I}}} \approx 1$, $\Theta_{\beta_{\mathrm{I}}} \approx 1$, $\Theta^a_{\alpha_{\mathrm{II}}} \approx 2\frac{\alpha_{\mathrm{II}}}{a\omega}$ and $\Theta^a_{\beta_{\mathrm{II}}} \approx 2\frac{\beta_{\mathrm{II}}}{a\omega}$, in the solution (164), and after some algebraic manipulation, the expression for the first extensional mode in terms of material properties is

$$
\begin{aligned}
V_E &= \sqrt{\frac{\beta_{\rm c}^2(3\alpha_{\rm c}^2+4\beta_{\rm c}^2)}{\alpha_{\rm c}^2-\beta_{\rm c}^2}} - \\
&\quad {\rm i}\frac{1}{2}\left\{\left(\underline{\frac{2\,{\rm d_f}\,{\rm H_0}\,\alpha_{\rm fl}^2\,(3\,\alpha_{\rm c}^2-8\,\beta_{\rm c}^2)}{3\,{\rm H_c}\,(3\,\alpha_{\rm c}^2+4\,\beta_{\rm c}^2)}} + \underline{\frac{{\rm d_f}\,{\rm m_f}\,\beta_{\rm c}^2(-4\,\beta_{\rm c}^2+\alpha_{\rm c}^2(-2\,\lambda_2+\lambda_1(2+\lambda_2)))}{3(\alpha_{\rm c}^2-\beta_{\rm c}^2)}}\right.\right. \\
&\quad \left.\left. -a\,\omega\frac{{\rm d_f}\,{\rm m_f}(2\,\alpha_{\rm c}^2\,\beta_{\rm c}^2(\lambda_1-\lambda_2)+\alpha_{\rm c}^4\,\lambda_1\,\lambda_2-2\,\beta_{\rm c}^4(\lambda_1-\lambda_2+4\,\lambda_1\,\lambda_2))}{6\,(\alpha_{\rm c}^2-\beta_{\rm c}^2)^2}\right)\frac{\omega}{\Omega_i}\right. \\
&\quad \left. -\left(\frac{\alpha_\mu\,\beta_{\rm c}^2(\alpha_{\rm c}^4\,(3+2\,\lambda_1)-2\,\alpha_{\rm c}^2\,\beta_{\rm c}^2\,(\lambda_1-2)-\,{\rm a}\,\omega\,\lambda_1\,(\alpha_{\rm c}^2-\beta_{\rm c}^2))}{3\,(\alpha_{\rm c}^2-\beta_{\rm c}^2)^2}\right)\frac{\omega}{\Omega_\beta}\right\},
\end{aligned}
\tag{183}
$$

with

$$
\lambda_1 = 1-\frac{\alpha^\star}{\eta_0}\,\frac{\alpha_{\rm fl}^2}{\alpha_{\rm c}^2}, \tag{184}
$$

$$
\lambda_2 = 1-\frac{\alpha}{\eta_0}\,\frac{\alpha_{\rm fl}^2}{\alpha_{\rm c}^2}, \tag{185}
$$

where the phase velocity ($\mathbf{Re}(V_E)$) correspond to the Gassmann effective elastic medium, and the attenuation is obtained by the expression

$$
\frac{1}{\rm Q} = -2\frac{\mathbf{Im}(V_E)}{\mathbf{Re}(V_E)}. \tag{186}
$$

The approximation for the fast extensional wave is plotted in Figure (7). It is remarkable that the attenuation is a precise fit using the leading two, underlined, terms of the imaginary part to plot expression (183).

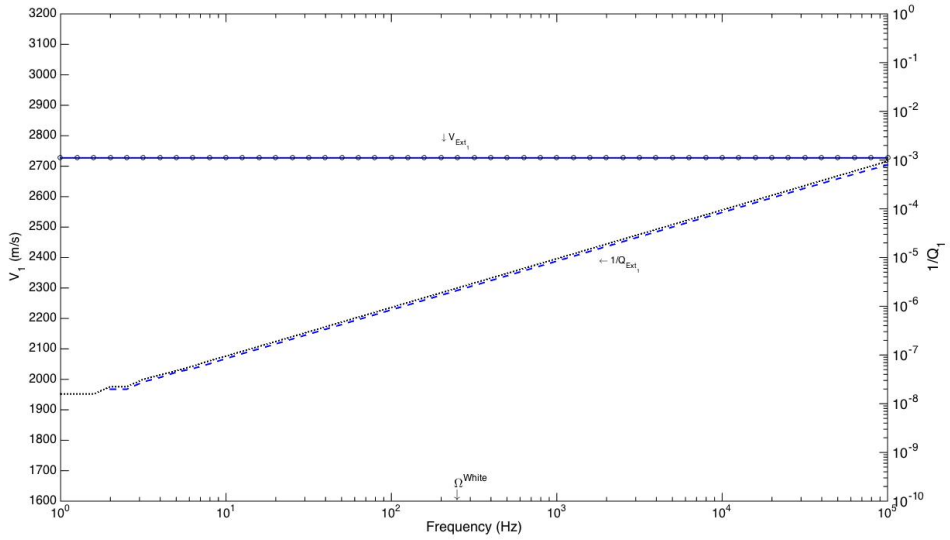

Figure 7: Asymptotes for the first extensional mode for closed-pore case. The exact phase velocity and attenuation of the first mode are shown by the blue solid- and dash- line, respectively. Its approximations for phase velocity (empty circles) and attenuation (dot-line) are plotted in black

Chapter 7 Conclusions

Based on the dCS theory, I have solved the extensional problem of a poroelastic cylinder with impermeable surface. For this, the boundary conditions for a stress-free impermeable surface are taken as the following:

i) vanishing total stress,

ii) no relative motion of the fluid with respect to the solid in the normal direction and

iii) no internal stress in the tangential direction.

This set is an adjoint boundary condition of the dCS wave operator.

With these boundary conditions, the dispersion relation is established, whose solution shows that a saturated porous cylinder apart from being like an effective elastic solid, as considered in the experimental community, has two additional modes.

The first mode, a fast-extensional mode, has a phase velocity corresponding to an undrained extensional modulus, and negligible attenuation that is also linearly frequency dependent.

The second mode is the result of the interaction between slow P and slow S waves. This mode is highly dissipative, such that it dampens within a minuscule fraction of the excitation cycle.

The third mode is essentially a slow P wave. This mode is very attenuated, its amplitude decreases by a factor of $e^{-\pi}$ in half a cycle.

The asymptotic analysis of the fast-extensional mode shows that the phase velocity of this corresponds to the undrained extensional modulus.

Due to the confining pressure applied to seal a sample in a LF experiment, a sealed porous cylinder is subjected to oscillations under the conditions of stress on its radial surface. Therefore, instead of excitation of the first extensional mode exclusively, other two natural modes are also induced in the sample. The unexplained observed loss of energy in LF experiments are due to the presence of those two highly attenuated modes. I plan to work on the quantitative modeling of the observed attenuations in the LF experiments using these modes. Also, I intend to further examine the significance of the impermeable boundary conditions used in this study; in particular, its effect on the reflection and transmission of seismic wave fields.

Cited literature

Al-Tahini, A. M., Abousleiman, Y. N., & Brumley, J. L. (2005). Acoustic and quasistatic laboratory measurement and calibration of the pore pressure prediction coefficient in the poroelastic theory. En: *SPE Annual Technical Conference and Exhibition*. Society of Petroleum Engineers.

Anderson, T. & Jackson, R. (1967). A fluid mechanical description of fluidized beds. *Industrial & Engineering Chemistry Fundamentals*, **6**(4): 527–539.

Batzle, M. L., Han, D.-H., & Hofmann, R. (2006). Fluid mobility and frequency-dependent seismic velocity—direct measurements. *Geophysics*, **71**(1): N1–N9.

Berryman, J. G. (1983). Dispersion of extensional waves in fluid-saturated porous cylinders at ultrasonic frequencies. *The Journal of the Acoustical Society of America*, **74**(6): 1805–1812.

Berryman, J. G. (1992). Effective stress for transport properties of inhomogeneous porous rock. *Journal of Geophysical Research: Solid Earth*, **97**(B12): 17409–17424.

Best, A., McCann, C., & Sothcott, J. (1994). The relationships between the velocities, attenuations and petrophysical properties of reservoir sedimentary rocks. *Geophysical Prospecting*, **42**(2): 151–178.

Biot, M. A. (1956). Theory of propagation of elastic waves in a fluid-saturated porous solid. i. low-frequency range. *The Journal of the acoustical Society of america*, **28**(2): 168–178.

Biot, M. A. (1962). Mechanics of deformation and acoustic propagation in porous media. *Journal of applied physics*, **33**(4): 1482–1498.

Birch, F. & Bancroft, D. (1938). Elasticity and internal friction in a long column of granite. *Bulletin of the Seismological Society of America*, **28**(4): 243–254.

Blöcher, G., Reinsch, T., Hassanzadegan, A., Milsch, H., & Zimmermann, G. (2014). Direct and indirect laboratory measurements of poroelastic properties of two consolidated sandstones. *International Journal of Rock Mechanics and Mining Sciences*, **67**: 191–201.

Born, W. (1941). The attenuation constant of earth materials. *Geophysics*, **6**(2): 132–148.

Bourbié, T., Coussy, O., & Zinszner, B. (1987). Acoustics of porous media: Editions technip.

Brown, R. J. & Korringa, J. (1975). On the dependence of the elastic properties of a porous rock on the compressibility of the pore fluid. *Geophysics*, **40**(4): 608–616.

de la Cruz, V. & Spanos, T. (1985). Seismic wave propagation in a porous medium. *Geophysics*, **50**(10): 1556–1565.

de la Cruz, V. & Spanos, T. (1989a). Seismic boundary conditions for porous media. *Journal of Geophysical Research: Solid Earth*, **94**(B3): 3025–3029.

de la Cruz, V. & Spanos, T. (1989b). Thermomechanical coupling during seismic wave propagation in a porous medium. *Journal of Geophysical Research: Solid Earth*, **94**(B1): 637–642.

De La Cruz, V., Sahay, P., & Spanos, T. (1993). Thermodynamics of porous media. En: *Proceedings of the Royal Society of London A: Mathematical, Physical and Engineering Sciences*. The Royal Society, Vol. 443, pp. 247–255.

Deresiewicz, H. & Skalak, R. (1963). On uniqueness in dynamic poroelasticity. *Bulletin of the Seismological Society of America*, **53**(4): 783–788.

Dunn, K.-J. (1986). Acoustic attenuation in fluid-saturated porous cylinders at low frequencies. *The Journal of the Acoustical Society of America*, **79**(6): 1709–1721.

Dunn, K.-J. (1987). Sample boundary effect in acoustic attenuation of fluid-saturated porous cylinders. *The Journal of the Acoustical Society of America*, **81**(5): 1259–1266.

Friedman, B. (1962). *Principles and techniques of applied mathematics*. Wiley New York.

Gardner, G., Wyllie, M., & Droschak, D. (1964). Effects of pressure and fluid saturation on the attenuation of elastic waves in sands. *Journal of Petroleum Technology*, **16**(02): 189–198.

Garnder, G. H. F. (1962). Extensional wave in fluid-saturated porous cylinders. *The Journal of the Acoustical Society of America*, **34**(1): 36–40.

Golub, G. H. & Van Loan, C. F. (1996). *Matrix computations, 3rd*. Johns Hopkins Univ Press.

Gurevich, B. & Schoenberg, M. (1999). Interface conditions for Biot's equations of poroelasticity. *The Journal of the Acoustical Society of America*, **105**(5): 2585.

Hart, D. J. & Wang, H. F. (2010). Variation of unjacketed pore compressibility using gassmann's equation and an overdetermined set of volumetric poroelastic measurements. *Geophysics*, **75**(1): N9–N18.

Hickey, C., Spanos, T., & De La Cruz, V. (1995). Deformation parameters of permeable media. *Geophysical Journal International*, **121**(2): 359–370.

Jackson, I., Paterson, M., Niesler, H., & Waterford, R. (1984). Rock anelasticity measurements at high pressure, low strain amplitude and seismic frequency. *Geophysical Research Letters*, **11**(12): 1235–1238.

Jackson, I., Schijns, H., Schmitt, D. R., Mu, J., & Delmenico, A. (2011). A versatile facility for laboratory studies of viscoelastic and poroelastic behaviour of rocks. *Review of Scientific Instruments*, **82**(6): 064501.

Johnson, D. L. & Kostek, S. (1995). A limitation of the biot–gardner theory of extensional waves in fluid-saturated porous cylinders. *The Journal of the Acoustical Society of America*, **97**(2): 741–744.

Krebes, E. & Daley, P. (2007). Difficulties with computing anelastic plane-wave reflection and transmission coefficients. *Geophysical Journal International*, **170**(1): 205–216.

Liu, H.-P. & Peselnick, L. (1983). Investigation of internal friction in fused quartz, steel, plexiglass, and westerly granite from 0.01 to 1.00 hertz at 10- 8 to 10- 7 strain amplitude. *Journal of Geophysical Research: Solid Earth*, **88**(B3): 2367–2379.

Madonna, C. & Tisato, N. (2013). A new seismic wave attenuation module to experimentally measure low-frequency attenuation in extensional mode. *Geophysical Prospecting*, **61**(2): 302–314.

Marle, C. (1967). Ecoulements monophasiques en milieu poreux. *Rev. Inst. Francais du Petrole*, **22**(10): 1471–1509.

Nur, A. & Byerlee, J. (1971). An exact effective stress law for elastic deformation of rock with fluids. *Journal of Geophysical Research*, **76**(26): 6414–6419.

Pimienta, L., Fortin, J., & Guéguen, Y. (2015). Bulk modulus dispersion and attenuation in sandstones. *Geophysics*.

Pimienta, L., Fortin, J., & Guéguen, Y. (2017). New method for measuring compressibility and poroelasticity coefficients in porous and permeable rocks. *Journal of Geophysical Research: Solid Earth*, **122**(4): 2670–2689.

Plona, T. J. (1980). Observation of a second bulk compressional wave in a porous medium at ultrasonic frequencies. *Applied Physics Letters*, **36**(4): 259–261.

Press, W. H., Teukolsky, S. A., Vetterling, W. T., & Flannery, B. P. (1996). *Numerical recipes in C*, Vol. 2. Cambridge university press Cambridge.

Sahay, P. N. (1996). Elastodynamics of deformable porous media. En: *Proceedings of the Royal Society of London A: Mathematical, Physical and Engineering Sciences*. The Royal Society, Vol. 452, pp. 1517–1529.

Sahay, P. N. (2001). Dynamic green's function for homogeneous and isotropic porous media. *Geophysical Journal International*, **147**(3): 622–629.

Sahay, P. N. (2008). On the biot slow s-wave. *Geophysics*, **73**(4): N19–N33.

Sahay, P. N. (2013). Biot constitutive relation and porosity perturbation equation. *Geophysics*.

Sahay, P. N., Spanos, T. T., & De La Cruz, V. (2001). Seismic wave propagation in inhomogeneous and anisotropic porous media. *Geophysical Journal International*, **145**(1): 209–222.

Senior, T. (1960). A note on hansen's vector wave functions. *Canadian Journal of Physics*, **38**(12): 1702–1705.

Solorza, S. & Sahay, P. N. (2009). On extensional waves in a poroelastic cylinder within the framework of viscosity-extended Biot theory: The case of traction-free open-pore cylindrical surface. *Geophysical Journal International*, **179**(3): 1679–1702.

Spencer, J. W. (1981). Stress relaxations at low frequencies in fluid-saturated rocks: Attenuation and modulus dispersion. *Journal of Geophysical Research: Solid Earth*, **86**(B3): 1803–1812.

Spencer, J. W. & Shine, J. (2016). Seismic wave attenuation and modulus dispersion in sandstones. *Geophysics*, **VOL. 81,**(NO. 3): D211–D231.

Subramaniyan, S., Quintal, B., Tisato, N., Saenger, E. H., & Madonna, C. (2014). An overview of laboratory apparatuses to measure seismic attenuation in reservoir rocks. *Geophysical Prospecting*, **62**(6): 1211–1223.

Tisato, N. & Madonna, C. (2012). Attenuation at low seismic frequencies in partially saturated rocks: Measurements and description of a new apparatus. *Journal of Applied Geophysics*, **86**: 44–53.

Tittmann, B., Nadler, H., Clark, V., Ahlberg, L., & Spencer, T. (1981). Frequency dependence of seismic dissipation in saturated rocks. *Geophysical Research Letters*, **8**(1): 36–38.

Toksöz, M., Johnston, D. H., & Timur, A. (1979). Attenuation of seismic waves in dry and saturated rocks: I. laboratory measurements. *Geophysics*, **44**(4): 681–690.

Whitaker, S. (1967). Diffusion and dispersion in porous media. *AIChE Journal*, **13**(3): 420–427.

White, J. E. (1986). Biot-Gardner porous rods theory of extensional waves in. *Society*, **51**(3): 742–745.

Winkler, K. & Nur, A. (1979). Pore fluids and seismic attenuation in rocks. *Geophysical Research Letters*, **6**(1): 1–4.

Winkler, K. W. (1983). Frequency dependent ultrasonic properties of high-porosity sandstones. *Journal of Geophysical Research: Solid Earth*, **88**(B11): 9493–9499.